Characterization of blood flow in the retinal vascular network

A DISSERTATION
SUBMITTED TO THE FACULTY OF
THE UNIVERSITY OF MINNESOTA
BY

Tess Ellen Kornfield

IN PARTIAL FULFILLMENT OF THE REQUIREMENTS
FOR THE DEGREE OF
DOCTOR OF PHILOSOPHY

Advisor: Eric A. Newman

January 2015

Acknowledgements

I thank my advisor Eric Newman for his excellent mentorship, unfailing support, and for his eternal optimism.

I thank my fellow Newman Lab students for the help, encouragement, friendship, and thoughtful conversations. Kyle Biesecker, Joanna Kur, Anusha Mishra, and Anja Srienc: you are all wonderful.

I thank Mike Burian for his steady surgical hands and his invaluable assistance in all aspects of lab life.

I thank my committee members Paulo Kofuji, Steve McLoon, and Noam Harel for their many helpful suggestions and contributions to my dissertation project. I especially acknowledge Dr. Kofuji for generously providing me immunohistochemistry protocols and reagents.

I thank Jan Dubinsky and Linda McLoon for their generosity of spirit and resources, and for their enthusiastic support of my endeavors both in and out of the lab.

Portions of this work have been previously published in *The Journal of Neuroscience* (Kornfield and Newman, 2014, Chapter 4); I thank David Attwell, Anna Devor, and Anusha Mishra for their comments on the manuscript, Michael Burian for his invaluable technical assistance, and Kyle Biesecker, Michael Burian, Joanna Kur, and Anja Srienc for their helpful discussions and for reviewing the manuscript.

Dedication

I dedicate this dissertation to my family and heartfriends who have helped make the last five and a half years fulfilling and joyful. Let us share our successes!

Table of Contents

List of Tables

List of Figures

Chapter 1: Introduction

Brain function is critical for survival. The oxygen and metabolic substrates required to maintain normal brain activity are delivered via a dense network of blood vessels that readily react to neuronal activity. The questions explored here focus on the retina, a part of the central nervous system (CNS), where the vascular network can be easily visualized and neuronal activity can be elicited with light.

The primary goal of the work presented here is to understand how blood flow is regulated in the retinal vascular network in response to neuronal activity. In order to accurately quantify blood flow, we developed a multitude of streamlined techniques capable of measuring relative and absolute vessel diameter, blood flow, blood cell flux, and blood velocity. We applied these techniques in the in vivo rat retina by 1) adding a dye to the blood plasma, allowing for intralaminar diameter measurement, and 2) by injecting fluorescently labeled red blood cells (RBCs) into the circulatory system. Tracking these fluorescent cells allowed us to measure numerous blood flow parameters, often simultaneously with the diameter measurements. These techniques were applied in retinal vessels of all sizes, from the smallest capillaries to the largest venules.

The aforementioned techniques were used to investigate retinal functional hyperemia, defined as the increase in local blood flow that occurs in response to nearby neuronal activity. Although large arteries and arterioles are known to dilate in response to synaptic activity, no other published work has investigated the magnitude and timing of the functional hyperemia response as it presents in the different compartments of the retinal vascular network. By doing a comprehensive survey of all retinal vessels, we aim to determine which vessels drive blood flow changes in the retina. Further, retinal capillaries are known to dilate in response to neuronal activity, but the source of their increase in blood flow remains unclear. Capillary blood flow may be regulated independently of large upstream vessels, potentially by contractile cells called pericytes that dot capillary walls. Complicating the picture is that the retina is a tri-laminar vascular structure, and blood flow in each of the three layers could be regulated independently

according to the metabolic needs of nearby neurons. The work in this dissertation addresses these questions and informs our understanding of blood flow regulation within the retinal vascular network.

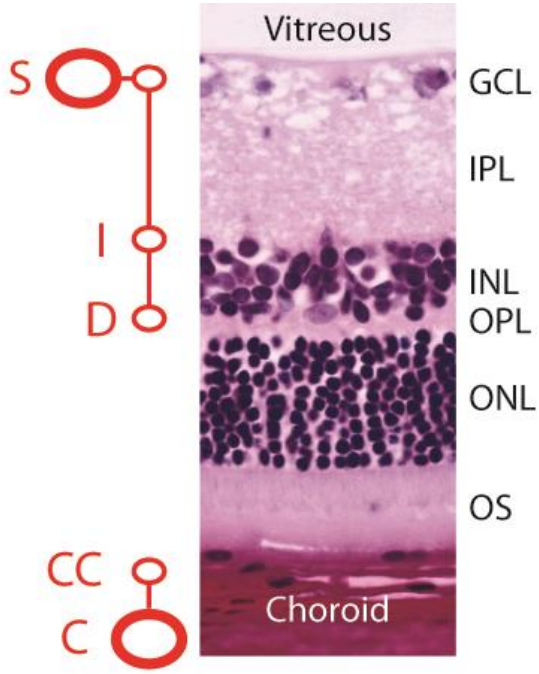

Figure 1.1. Schematic of the retinal vascular networks relative to the retinal neuronal layers. The trilaminar retinal vascular network is composed of the superficial (S), intermediate (I), and deep (D) vascular layers. The choroidal vascular network is composed of large choroidal vessels (C) and the choriocapillaris (CC). GCL, Ganglion cell layer; IPL, inner plexiform layer; INL, inner nuclear layer; OPL, outer plexiform layer; ONL, outer nuclear layer; PR, photoreceptors.

Retinal vascular morphology

The mammalian retina is a complex laminar neural tissue that forms from the diencephalon during embryonic development. The retinal tissue of many higher mammals including the human, rat, mouse, and cat, is nourished by two separate vascular systems: the choroidal and the retinal vasculature (Fig. 1.1). Some animals, such as the rabbit and guinea pig, have avascular inner retinas and rely solely on diffusion from the choroidal circulation to meet the retina's metabolic requirements (Yu and Cringle, 2001), but this configuration will not be discussed here. The outer retina is oxygenated by the

choroid, a layer of vascularized connective tissue that becomes continuous with the arachnoid and pia at the optic nerve. The choroid includes a fenestrated and dense network of capillaries called the choriocapillaris, which lies between the retina and the sclera. Oxygen from the choroid reaches photoreceptors by diffusing across Bruch's membrane and the retinal pigment epithelium. Blood flow in the choroid is one of the highest in the body, accounting for 65-85% of the blood flow to the retina (Bill et al., 1983). This high blood flow is necessary, in part, due to the high metabolic rate of photoreceptors. The other vascular system, which is of primary interest here, is called the retinal vasculature. It provides oxygen to the inner retinal layers.

The retinal vascular network originates as a branch of the ophthalmic artery and emerges from the central retinal artery at the optic disc, splitting into arterioles that traverse the retinal surface adjacent to the vitreous humor. Blood exits the retina via primary venules that lie at the retinal surface and merge at the optic disc to become the primary retinal vein. The vascular tree that connects retinal arterioles to venules is a stratified structure that is composed of three planar layers at distinct depths (Fig. 1.1). The morphology and connectivity of this trilaminar network has been previously described (Paques et al., 2003) and modeled (Ganesan et al., 2010, 2011). The superficial vascular layer is made up of venules, and arterioles and their branches. This layer is in the retinal ganglion cell layer and provides oxygen and nutrients primarily to retinal ganglion cells. As the arterioles branch, the daughter vessels become narrow and are classified as capillaries. Capillaries of the superficial vascular layer then dive into the retinal tissue, away from the vitreous humor, to form the intermediate vascular layer, a layer of sparse and narrow capillaries that lies at the border of the inner plexiform layer and inner nuclear layer. Intermediate layer capillaries traverse for only a short distance before diving further into the retina to form the deep vascular layer. The deep vascular layer is a dense and highly interconnected meshwork of capillaries at the border of the inner nuclear layer and the outer plexiform layer. Draining venules are present in the deep vascular layer, which ascend and connect to surface layer venules, delivering deoxygenated blood out of the retina. During development, the intermediate and then deep vascular layers sprout from the superficial vascular layer (Provis, 2001).

Blood percolates through the three retinal vascular layers roughly in series. Blood entering the retina via the arterioles first flows through the superficial vascular layer, then through the intermediate vascular layer, then down to the deep vascular layer, and then drains from the eye through the venules. Morphological studies have estimated that around 70% of blood that enters the eye goes through all three layers before exiting (Paques et al., 2003). This indicates that 30% of blood takes the opportunity to bypass the deep and/or intermediate vascular layers, although more work is required to track the path of blood through the network. An arterio-venous shunt in the superficial vascular layer connects superficial layer capillaries with primary venules. Intermediate layer capillaries can also connect directly to ascending venules, allowing blood to bypass the deep vascular layer. Although the structure of the retina's trilaminar vascular network has been described, our work is the first to investigate differences in blood flow between the three layers.

Vessel classification is difficult, as biological complexity is not easily distilled into objective categories. Many methods for blood vessel classification have been developed to address this problem. They take into consideration a combination of branch pattern, branch angle, and vessel diameter, length, and density. Strahler's method is a popular way of characterizing branching complexity. It was originally developed to classify branching streams and has since been applied to many biological systems with hierarchical organization including trees, pulmonary airways, and vascular networks (Cassot et al., 2006; Lapi et al., 2008). A Strahler's number of one is assigned to the most downstream segment and, moving upstream, the order number increases as segments merge. When Strahler's method was applied to blood vessels, it was updated to take vessel diameter into account (Kassab et al., 1997). Another classification method is graph analysis, where vessel connection points are represented as "nodes" and vessel segments as "edges." This method has been used to classify cerebral vascular systems (Blinder et al., 2013; Lindvere et al., 2013; Reichold et al., 2009). Fractal analysis has also been used to model vascular networks (Lorthois and Cassot, 2010; Risser et al., 2007). The gamut of methods available for characterizing cerebral vascular topology, and their application in interpreting blood flow data, have been thoroughly reviewed (Hirsch et al., 2012).

The classification system employed here is based solely on branch order and retinal depth. In the superficial vascular layer, a hierarchical classification system is used. Primary arterioles are designated as order 1 and each branching point increments the order by 1. The term "capillary" has a fraught definition, but for our purposes vessels in the superficial layer of order 4 and higher are defined as capillaries (see Chapter 4 for more detail). Classifying branching vessels by order allows us to describe them in a biologically meaningful way. However, it is important not to overstate the value of order; because the vascular system shifts from the arterial to venular side slowly without any hard cutoffs and there is wide biological variation in vascular networks, order is used only as a guide. The intermediate and deep vascular layers lack a hierarchical branching pattern and can be modeled more accurately using meshes with different densities (Ganesan et al., 2010, 2011). We classify all vessels in the intermediate and deep vascular layers as capillaries, except for draining venules in the deep vascular layer, which were not investigated. It should be noted that discrepancies between vessel classification methods might account in part for differences in our results and data from other laboratories.

The retina's oxygen profile resembles a U due to its dual oxygen sources. The partial pressure of oxygen (pO_2) is highest at the retina's edges, where oxygen diffuses into the inner retina from the vitreous humor and the large vessels of the retinal vasculature, and into the outer retina from the choroidal vasculature. pO_2 dips to nearly hypoxic levels in the middle of the retina (Alder et al., 1983; Lau and Linsenmeier, 2012; Linsenmeier and Padnick-Silver, 2000; Yu et al., 1994). However, the intermediate and deep vascular layers provide oxygen sources at the borders of the inner nuclear layer. Using oxygen-sensitive electrodes to measure oxygen concentration through the retina's depth, studies find evidence of a bump in pO_2 near the deep vascular layer (Yu and Cringle, 2001; Yu et al., 1994) and near both the intermediate and deep vascular layers during light adaptation (Lau and Linsenmeier, 2012; Linsenmeier, 1986). The fact that we can detect the presence of retinal vascular layers by measuring oxygen shows that the intermediate and deep vascular layers are functional and provide valuable metabolic support to the middle of the retina.

Vascular density tends to correlate with overall neuronal activity. This is true in the cortex, where the highest vascular density is in layer IV, which also has the highest cytochrome oxidase activity (Weber et al., 2008). In the retina, we expect the position of the three vascular layers to correspond with neuronal metabolic requirement. The oxygen requirements of different retinal neurons vary with changes in luminance and in response to other light stimuli. Photoreceptors hyperpolarize in response to light, so oxygen requirements are highest in the dark and lowest in bright light. The presence of parallel ON and OFF pathways means that bipolar and retinal ganglion cells have either high or low synaptic activity and oxygen requirements in light. There is evidence that oxygen consumption is highest in the OFF sublamina of the inner plexiform layer (Yu and Cringle, 2001), which is deeper than the ON sublamina and close to the intermediate vascular layer. Compared to photoreceptors, bipolar cells, and retinal ganglion cells, amacrine cell have a complex synaptic connectivity profile. Amacrine cell synapses make up the vast majority of synapses in the inner plexiform layer (Dowling, 1968). In aggregate, amacrine cells increase their activity in response to a flickering light, potentially drawing on oxygen delivered by the intermediate vascular layer. The work presented here dovetails with research characterizing retinal neuronal activity and oxygen uptake throughout the retinal profile, and implies that neuronal activity influences blood flow by vascular layer.

Principles of blood flow

The mathematical underpinnings of fluid flow have been studied for hundreds of years. A complete discussion of these principles is beyond the scope of this dissertation. However, accurately interpreting the results presented requires a basic understanding of blood flow dynamics. One of the most important equations characterizing the properties of blood flow is the Hagen-Poiseuille equation, which relates flow to the pressure difference between the two ends of a tube, its cross-sectional area, and the fluid viscosity. This equation has a variety of applications, and has been tweaked over the years to more accurately characterize blood flow by accounting for the non-ideal nature of blood and blood vessels. One important concept arising from the Hagen-Poiseuille equation is that

vessel resistance is inversely proportional to the fourth power of the vessel radius. Further, flow is proportional to the fourth power of the vessel radius. Because blood flow is very sensitive to changes in vessel width, we take care to measure diameter with high precision.

For an ideal fluid flowing through an ideal tube, laminar flow mandates that velocities will be highest in the center of the tube and will approach zero at the tube's edges. The distribution of flow velocities across the width of this tube is parabolic. However, as much as we might like them to be, blood vessels are not ideal tubes. They are tortuous, interconnected, branching things with a range of sizes. Nor is blood is a Newtonian fluid; it is pulsatile, particulate, and viscous. In the case of a particulate substance such as blood, particle density is non-uniform across tube's width. Particulate components tend to compact densely at the tube's center, a phenomenon called axial streaming. The result of axial streaming in blood vessels is that the blood components separate, creating a low-viscosity layer of cell-free plasma at the vessel's edges and a high-viscosity bulk of blood cells at the center. Therefore, most investigations of laminar flow in vivo find that parabolic profiles are blunted (Logean, Eric and Schmetterer, 2003; Parthasarathi et al., 1999; Rovainen et al., 1993; Zhong et al., 2011). Although flow velocities of zero have been measured at the edges of vessels (Yazdanfar et al., 2003; Zhi et al., 2011), this is unusual and likely depends on the measurement technique. Techniques that measure the velocity of cells cannot capture velocities in the cell-free regions, a methodological drawback that we cannot as yet overcome. Perfect parabolas representing velocity across a vessel's width are disrupted near branch points (Logean, Eric and Schmetterer, 2003; Willerslev et al., 2014; Zhong et al., 2011). Further, whether laminar flow is present depends on vessel diameter. With decreasing vessel diameter, each individual blood cell will take up proportionally more space in the lumen. This also increases the frictional forces between cells and the vessel wall, disrupting laminar flow. In vessels where RBCs move single-file, RBCs that are normally 8 μm wide biconcave disks deform into bullet-shaped objects, thanks to their liquid centers (Fung, 1969), in order to squeeze through the lumen. Here, laminar flow is not a useful model for interpreting blood velocity. In our experiments we measure parabolic profiles in vessels

between 20 and 30 μm in diameter and use this result as a readout to confirm our ability to measure accurate flow velocities in retinal vessels. These results will be discussed in Chapter 3.

Properties of blood flow change as the blood moves from large to small vessels. These properties are in part mediated by the presence of glycocalyx, also called the endothelial surface layer. Glycocalyx is a glycoprotein and proteoglycan layer lining the luminal side of the vascular endothelium. It is approximately 0.5 μm thick and repels cells from the edges the vessel, impedes plasma flow, and is partially responsible for generating the ever-present cell-free plasma layer at vessel edges (its many effects are reviewed by Reitsma et al (2007)). As vessel diameters decrease, the cell-free plasma layer takes up proportionally more of the lumen, causing the effective blood viscosity to decrease, a phenomenon called the Fahraeus-Lindqvist effect. A related phenomenon is the Fahraeus effect, defined as the decrease in hematocrit that accompanies decreasing diameter. In interpreting the results presented here, we must keep in mind that the parameters that constrain blood flow are not constant throughout the vascular network.

RBCs are the body's quantal unit of oxygen delivery, and tracking their flow allows us to infer energy delivery to nearby tissues. High-resolution phosphorescence lifetime microscopy can be used to visualize the high oxygen signals associated with individual RBCs moving through capillaries (Parpaleix et al., 2013) and to measure blood flow in a vascular network (Shahidi et al., 2006, 2009; Wanek et al., 2011). By measuring RBC flux directly (Chapter 3), our experiments indirectly gauge tissue oxygenation at the level of individual blood vessels. Further, our measurements of RBC movement through vessels were used to validate important basic concepts of blood flow, including the existence of parabolic flow in the arterioles of the rat retina.

Functional hyperemia

Functional hyperemia was first described by Mosso in 1880 (Mosso, 1880) and was further characterized by Roy and Sherrington in 1890 (Roy and Sherrington, 1890). They brilliantly observed that the brain is capable of regulating its own blood supply. This simple observation has blossomed into a rich line of research into the underpinnings

of cerebral blood flow modulation. The body maintains physiologically normal blood flow and oxygenation on a global scale via autoregulation, which is accomplished by modulating cardiac output and the resistance of large blood vessels to account for changing blood pressure. On a smaller spatial scale, functional hyperemia couples neuronal activity to local blood flow increases. Its presence is critical for tailoring blood flow to areas of greatest need. In the brain, the body's most bloodthirsty organ, oxygen is critical for survival; oxygen levels rarely drop into the hypoxic. Functional imaging data demonstrates that neuronal activity causes paradoxical increases in blood oxygenation that exceed neuronal need (reviewed by Paulson et al (2010)). These oxygen overshoots are thought to prevent brain tissue distant from blood vessels from becoming hypoxic (Devor et al., 2011). Because oxygen delivery to the CNS is critical, redundant mechanisms control the functional hyperemia response. It is important that we understand the biological basis of functional neuroimaging, as it is currently the best way to non-invasively measure human brain activity in real time. Further, understanding the pathways behind functional hyperemia will open doors for treatment options in diseases where blood flow is disrupted.

The link between neuronal activity and blood flow is mediated by complex signaling pathways that are incompletely understood. Although vasoactive signals have numerous origins, the primary targets of their action are vascular smooth muscle cells (SMCs), which directly modulate the diameter of large arterial-side blood vessels. The contribution of pericytes to regulation of capillary diameter will be discussed in the next section. SMCs surround the endothelial cell wall of arteries and arterioles in the CNS, sometimes creating multiple layers in the largest blood vessels. They wrap circumferentially around blood vessels, separated from underlying endothelial cells by a thin basement membrane (Gerhardt and Betsholtz, 2003). Vascular SMC constriction occurs when increases in the intracellular calcium concentration triggers activation of myosin light chain kinase, which phosphorylates myosin light chain. Myosin light chain then interacts with α-SMA to generate contractile force. Relaxation occurs when calcium concentration drops and/or there is increased activity of myosin light chain phosphatase

(Webb, 2003). The extent of α-SMA expression is correlated with vessel contractility (Hinz et al., 2001; Schildmeyer et al., 2000; Tomasek et al., 2006).

Neuronal control of CNS vasculature is both long-range and local. In the brain, blood vessels are innervated by sympathetic and parasympathetic fibers, providing external control over blood flow largely for autoregulatory purposes (Hamel, 2006). In contrast, blood flow in the retinal vasculature is controlled by local rather than extrinsic signals. The central retinal artery is highly innervated by sympathetic and parasympathetic fibers, but these fibers are absent in the intraocular retinal vasculature (Bergua et al., 2003; Ye et al., 1990). Conflicting data suggest that autonomic machinery is present in the retina (Forster et al., 1987; Furukawa, 1987), and sympathetic denervation was associated with reduced vascular responsiveness in human retinas (Lanigan et al., 1990). Despite these opposing data, the dogma remains that local changes in retinal vascular tone originate from nearby cells. Retinal functional hyperemia begins when vasoactive signals are released directly from neurons during synaptic signaling events. Activation of postsynaptic glutamate receptors causes swift calcium elevations, activation of neuronal nitric oxide synthase, and release of the potent vasodilator nitric oxide (NO). Active neurons also release prostaglandin E2, which has a dilatory effect on the vasculature.

Glial cells are important mediators of neurovascular coupling. The primary glial cell in the brain is the astrocyte, and its functional analogue in the retina is the Müller cell. Astrocytes are only present at the retina's surface and therefore their influence is limited compared to Müller cells, which span the entire retinal depth. Glial cells of all types are uniquely well positioned to regulate blood flow. They are closely associated with pre- and post-synaptic structures as part of the tripartite synapse (Perea et al., 2009), and glial perivascular processes envelop blood vessels nearly completely (Mathiisen et al., 2010). Due to their synaptic and vascular contact points, glial cells can relay neuronal chatter to the vascular system. Extensive literature supports a role for glia in blood flow regulation (Attwell et al., 2010; Haydon and Carmignoto, 2006; Iadecola and Nedergaard, 2007; Newman, 2013). Mechanistically, presynaptic glutamate release activates metabotropic glutamate receptors on glial cells, increasing their cytosolic

calcium concentration and triggering the synthesis of vasoactive metabolites of arachidonic acid. Synaptic activity in the retina also leads to the release of ATP, which activates glial purinergic receptors and causes glial release of vasoactive agents. Despite many careful studies linking glial signaling and changes in blood flow, recent work using genetic techniques and next-generation calcium indicator molecules has questioned the role of glia in functional hyperemia. This work finds that blood flow responses are preserved in the absence of glial calcium signaling (Bonder and McCarthy, 2014; Nizar et al., 2013; Takata et al., 2013). Additional work is required to fully understand the role glial signaling plays in regulating blood flow.

Neuronally-evoked dilations spread along the vasculature, allowing for spatially limited neuronal activation to generate network-wide blood flow increases. Electrical signals propagate via gap junctionally connected endothelial cells, glial cells, and pericytes in the retina (Ishizaki et al., 2009; Peppiatt et al., 2006; Zhang et al., 2011) and other vascular networks. Of interest is the site of dilation initiation. In the cortex, sensory stimulation first triggers dilations in the deep cortical layers where capillaries and higher-order arteriole branches reside, which then spread toward the cortical surface (Chen et al., 2011; Hall et al., 2014; Silva and Koretsky, 2002; Tian et al., 2010). We aimed to identify the retinal vessel(s) that respond most quickly to neuronal signaling (Chapter 4). At stimulus offset, vessels constrict and blood flow returns to baseline. The return to baseline likely requires an active constriction rather than simply cessation of the dilatory signal (Chen et al., 2011). The biphasic functional hyperemia response we observe in the retina (Chapter 4) may be the result of an interaction between dilatory and constrictory signals with different temporal dynamics. Future pharmacological investigation could parse out these competing mechanisms.

Although the molecular underpinnings of functional hyperemia remain under active investigation, the functional hyperemia response is large, easily evoked, and consistent in the retinal vasculature and can be used to better understand how blood flow is regulated within a network. Further, functional hyperemia is often disrupted early in disease, causing a loss of blood flow to active tissues. In the retina, glaucoma and diabetic retinopathy disrupt blood flow regulation, which can cause catastrophic vision

loss (Garhöfer et al., 2004a; Mishra et al., 2010). Therefore, the functional hyperemia response is a potential therapeutic target, and understanding its expression in the retina vascular network is an important endeavor.

The role of pericytes in blood flow control

Pericytes were first named "Rouget cells" in 1873 for the man who characterized them, Charles-Marie Benjamin Rouget. Pericytes are mural cells that wrap around blood vessels in the CNS and throughout the body. Pericytes serve many diverse and important functions that have been thoroughly reviewed (Armulik et al., 2011; Dore-Duffy and Cleary, 2011; Krueger and Bechmann, 2010). They are critical for developing and maintaining normal microvascular architecture (Hellström et al., 2001) and for creating a functional blood-brain barrier (Armulik et al., 2010; Daneman et al., 2010; Kim et al., 2009; Winkler et al., 2012). Pericytes may also have pluripotent abilities (Diaz-Flores et al., 1992; Dore-Duffy, 2008; Dore-Duffy et al., 2006; Farrington-Rock et al., 2004), although this has not been demonstrated in vivo. Of particular interest here, pericytes have contractile properties (Joyce et al., 1985) and are thought to control microvasculature blood flow.

Mural cells are vascular-associated cells whose morphology shifts continuously along the vascular tree. Vascular SMCs and pericytes are both classified as mural cells, although their locations and morphologies differ dramatically. Vascular SMCs encircle and fully cover the surface of arterioles, and are still present but sparser on pre-capillary arterioles. Mural cells on capillaries are defined as pericytes. Pericyes have round cell bodies that protrude from the abluminal side of the blood vessel wall, primary processes that extend longitudinally along the vessel, and shorter secondary processes that wrap circumferentially around vessels. Pericyte somas appear intermittently along the vessel's length but their processes extend for long distances. Pericytes on pre-capillary vessels have processes that extend about 10 μm, while pericytes on capillaries have processes that extend ~ 30-40 μm (Borysova et al., 2013). Unlike vascular SMCs, which lie outside of the vascular basement membrane, healthy mature pericytes are enveloped between the inner and outer vascular basement membranes, making them physically part of the

vascular wall. On post-capillary venules pericytes are spidery, with stellate cell bodies and slender branching processes extending in all directions. Pericytes and vascular SMCs descend from the same lineage, and therefore no molecular marker can unequivocally tell them apart. Definitively identifying pericytes is only possible with ultrastructural analysis showing that the cell in question is within the vascular basement membrane, which is outside the realm of possibility for most researchers.

Pericytes are in contact with other cells, and their interactions may affect pericyte function. Astrocyte endfeet make contact with the vascular basement membrane and are close enough to signal to pericytes and other vascular cells. Pericytes and the underlying endothelial cells have numerous contact points and are connected via gap junctions. Further, the edges of pericyte processes are firmly anchored to endothelial cells at filamentous adhesion plaques for the transfer of contractile force. The signaling pathways between pericytes and endothelial have been reviewed by Gaengel et al (2009). Neuronal synaptic terminals are also closely apposed to pericytes, which can respond to neurotransmitters with changes in their intracellular calcium concentration (Kamouchi et al., 2004; Wu et al., 2003). Pericytes are also coupled to each other via gap junctions, suggesting that pericyte contractile or dilatory signals can propagate along the vessel wall (Wu et al., 2006).

Pericyte density varies across tissues and vascular beds. They are ubiquitous in the retinal vasculature, where their processes encapsulate approximately 96% of retinal vessels (Chan-Ling et al., 2011). In comparison, 11% of choroidal (Chan-Ling et al., 2011) and 37-80% of brain blood vessels (Mathiisen et al., 2010; Winkler et al., 2012) are covered by pericyte processes. The greater pericyte coverage in the retina compared to the brain (Cogan and Kuwabara, 1984; Frank et al., 1987) suggests differences in blood flow regulation between tissue types. Pericyte densities in the three retinal vascular layers have not been quantitatively assessed, although we observe them in all layers and particularly at branch points (unpublished findings). In the mouse retina's superficial vascular layer, pericyte density does not depend upon retinal eccentricity or quadrant (Schallek et al., 2013). The density of pericytes may affect blood flow regulation in the microvasculature (discussed further in Chapter 4).

Molecular markers are used to identify pericytes, although none is capable of definitively doing so at all stages of development. Commonly used pericyte markers include PDGFR-β, desmin, NG2, and α-SMA. Others have been proposed and are in need of validation (Armulik et al., 2011). Changes in the expression levels of these markers in the retina throughout development have been previously characterized (Hughes and Chan-Ling, 2004). NG2 is a common and useful marker for mature pericytes, and transgenic mice that express the fluorescent protein DsRed under the NG2 promoter have been used in recent studies to localize pericytes (Hall et al., 2014; Mishra et al., 2014; Schallek et al., 2013). However, the NG2-driven DsRed signal is strongest in somas and, particularly in vivo, pericyte processes cannot be clearly visualized (Hall et al., 2014; Schallek et al., 2013). The work presented here utilizes the NG2 antibody as a marker of pericyte somas in the rat retina.

Pericytes express contractile proteins and are capable of contracting and relaxing. The molecular contractile mechanisms of pericytes and vascular SMCs are very similar: both depend on modulation of intracellular calcium. Binding of vasocontrictive agents to nonspecific cation channels, or ATP to its receptors, depolarizes pericytes and raises their intracellular calcium concentration, generating constriction. Conversely, dilatory agents activate potassium channels, causing an efflux of potassium, hyperpolarization, and pericyte relaxation. Vasoactive substances can also act on intracellular cyclic nucleotide cascades that modulate ion channel activity, or by changing the phosphorylation state of proteins involved in muscular contraction pathways. The molecular mechanisms underlying pericyte contractility have been reviewed by Hamilton et al (2010).

One molecular species critical for generating pericyte contractility is α-SMA, a common actin isoform expressed in mural cells. As might be expected, α-SMA expression in vivo is on a continuum. Its expression is high in arterial vascular SMCs and decreases along the vascular tree until it becomes virtually absent on the smallest capillaries (Alliot et al., 1999; Boado and Pardridge, 1994; Hughes and Chan-Ling, 2004; Kornfield and Newman, 2014; Nehls and Drenckhahn, 1991). α-SMA is expressed in between 0 and 10% of pericytes in vivo and in acute cultures (Dore-Duffy and Cleary, 2011; Verbeek et al., 1994). Its expression is massively upregulated under culture

conditions (Verbeek et al., 1994), during inflammation (Pieper et al., 2014), in hypertension (Herman and Jacobson, 1988), and in tumors (Gerhardt and Betsholtz, 2003). Because of the low levels of actin expression in capillary pericytes in the healthy adult, it remains unclear how much contractile power these cells have in vivo.

Early pericyte observers noted their contractile properties and theorized about the role of pericytes in blood flow regulation. In vitro studies found that pericytes seeded on deformable beds wrinkled the underlying substrate and decreased its surface area; the story of these discoveries is nicely summarized by Krueger and Bechmann (2010). A large body of work shows that pericytes respond to a variety of vasoactive substances including adenosine (Li and Puro, 2001) and ATP (Peppiatt et al., 2006), dopamine (Wu et al., 2003), endothelin (Kawamura et al., 2002), acetylcholine (Wu et al., 2003), and angiotensin II (Kawamura et al., 2004). They are also sensitive to changes in pH (Chen and Anderson, 1997) and electrical stimulation (Peppiatt et al., 2006). Critical studies showed that pericytes can control the diameter of underlying capillaries (Dai et al., 2009; Peppiatt et al., 2006; Schönfelder et al., 1998; Yamanishi et al., 2006) and postcapillary venules (Borysova et al., 2013). However, in ex vivo experiments, only a subset of pericytes responds to contractile stimuli (Peppiatt et al., 2006). Pericytes' lack of actin expression and the narrow diameter of capillaries led many to conclude that blood flow regulation occurs at the level of the arteries and arterioles (Boas et al., 2008; Devor et al., 2007; Vanzetta et al., 2005).

The role of pericytes in regulating blood flow in vivo remains unclear. Capillaries account for up to 70% of the total vascular resistance (Boas et al., 2008), and even small changes in their diameter would have a huge effect on network blood flow. Loss of pericytes reduces the functional hyperemia response (Bell et al., 2010), although this could be due to their role maintaining blood vessel and blood-brain barrier integrity. Two studies investigating pericyte activity in vivo reported opposite results. First, using biccuculine to generate neuronal activity, cortical capillaries were shown to dilate in vivo, but the authors concluded that this was not an active response (Fernández-Klett et al., 2010). Second, using a physiological sensory stimulus, a different group observed pericyte-mediated capillary dilations, strongly suggesting they modulate blood flow in

vivo (Hall et al., 2014). Because of these opposing results, pericytes' role in blood flow control remains controversial. We have addressed this question in the retinal vasculature (Chapter 4).

Pericyte dysfunction has been implicated in a number of diseases. Changes in pericyte morphology or their coverage of capillaries have been observed in multiple sclerosis (Claudio et al., 1995; Kunz et al., 1995), epilepsy (Liwnicz et al., 1990), brain tumors (Winkler et al., 2004), and normal aging (Heinsen and Heinsen, 1983). Pericytes are thought to participate in β-amyloid clearance in Alzheimer's disease and die when exposed to β-amyloid (Verbeek et al., 1997; Wilhelmus et al., 2007). Pericyte death is an early hallmark of diabetic retinopathy (Beltramo and Porta, 2013; Cogan et al., 1961). Pericytes are very sensitive to hypoxia and ischemia causes them to die in rigor, constricting capillaries and preventing reperfusion of the microvasculature even if the original ischemic insult is removed (Peppiatt et al., 2006; Yemisci et al., 2009). After traumatic brain injury, pericyte constriction and death disrupts blood flow (Dore-Duffy et al., 2000, 2011). That pericytes are implicated in so many disease processes indicates their presence is critical for health and that they are potential therapeutic targets. Understanding their role in blood flow regulation in the healthy organism will provide clues into how blood flow is controlled on a network level and how to regain normal flow under pathological conditions.

Goals of this research

The goal of the present research is to understand how blood flow is controlled in the retinal vasculature: if blood flow is regulated differently in the three vascular layers, whether capillaries actively regulate blood flow, and how blood flow is regulated in the retinal vascular network as a whole. To answer these questions, we have developed methods to measure blood flow (Chapter 3) and applied them in an in vivo rat retinal preparation, where the functional hyperemia response was investigated at all levels of the trilaminar vascular network (Chapter 4).

Chapter 2: Methods

In vivo preparation.

The *in vivo* rat retinal preparation has been described previously (Srienc et al., 2012). All animals were treated in accordance with the University of Minnesota Institutional Animal Care and Use Committee guidelines. Briefly, 2 to 3-month-old male Long–Evans rats were anesthetized with isoflurane (2%), and the femoral artery and vein were cannulated for monitoring of blood pressure and injection of anesthetics and paralytics, respectively. A tracheotomy was performed. After surgery, the animal was anesthetized with α-chloralose (α-chloralose-HBC Complex; Sigma C8849; 800 mg/kg bolus and 550 mg/kg/h sustained infusion), and the paralytic gallamine triethiodide (Sigma G8134; 20 mg/kg bolus and 20 mg/kg/h sustained infusion) was administered to reduce eye movements. The paralytic agent did not affect the flicker-evoked vascular responses. A contact lens was placed over the eye. The animal was mounted in a custom stereotaxic holder that was attached to a stage, and the retina was imaged with a confocal microscope (Olympus FV1000) and a 4X dry 0.16 numerical aperture objective. A heating blanket was used to maintain the animal's body temperature at 37°C. The rat was ventilated (SAR-1000; CWE) with a mixture of 30% O_2 and 70% N_2 at 55 breaths/min with a tidal volume of ~3.4 ml, a 1:1 inspiration/expiration fraction, and 2 mmHg positive end-expiratory pressure. Oxygen saturation (sO_2; MouseOx; Starr Life Sciences), end-tidal CO_2 (microCapStar; CWE), and arterial blood pressure (Pressure Monitor BP-1; World Precision Instruments) were measured in real time. Carbon dioxide partial pressure (pCO_2), oxygen partial pressure (pO_2), and pH were sampled periodically (ABL800flex; Radiometer), and ventilation parameters were adjusted to maintain physiological parameters within normal limits (Table 2.1). Large tidal volume breaths up to 30 cmHg were given every ~5 min to maintain good lung ventilation. These breaths were often given immediately before blood sampling, accounting for the high pO_2 we observed in Chapter 4. If physiological parameters deviated from the normal range, the retinal functional hyperemia response was reduced or absent. Data were only collected when

parameters were within the normal range. After experimentation, animals were killed with an intravenous injection of potassium chloride (2 mEq/kg).

Table 2.1: Chapter 4 physiological parameters		
Physiological parameter	Mean ± S.E.M.	*N*
BP	120 ± 2 mmHg	46
pO_2	162 ± 4 mmHg	33
sO_2	94.8 ± 0.3%	46
pCO_2	32 ± 0.5 mmHg	33
pH	7.42 ± 0.00	33

Table 2.1. Chapter 4 physiological parameters. BP, mean arteriole blood pressure, pO_2, oxygen partial pressure; sO_2, oxygen saturation; pCO_2, CO_2 partial pressure; *N*, number of rats.

Fluorescent RBC labeling

RBCs were labeled with the lipophilic dye carbocyanide 1,1'-dioctadecyl-3,3,3',3'-tetramethylindodicarbocyanine, 4-chlorobenzenesulfonate salt (DiD solid; Invitrogen D-7757) using a procedure modified from Unthank et al. (1993). A total of 350 µl of blood was withdrawn from the arterial line, and RBCs were isolated by adding 700 µl of blood plasma buffer (BPB; in mM: 128 NaCl, 15 glucose, 10 HEPES, 4.2 $NaHCO_3$, 3 KCl, 2 $MgCl_2$, and 1 KH_2PO_4, pH 7.4; (Khoobehi et al., 2003)) and centrifuged for 5 min at 1500 rpm. RBCs were resuspended in 1.4 ml of BPB, and the cell suspension was gently mixed into a dye solution composed of 1.4 ml of Dilutent C (Sigma CGLDIL) and 35 µl of DiD (2.5 mg/mL in 100% ethanol). The solution was incubated for 5 min at 37°C with periodic inversion to ensure uniform labeling. After labeling, 700 µl of serum was added, and the solution was incubated for 1 additional minute. The fluorescent RBCs (fRBCs) were then centrifuged for 5 min at 1500 rpm and washed twice by gentle mixing in 3.5 ml of BPB containing 10% serum, followed by 5 min centrifugation at 1500 rpm to remove unbound dye. Washed and labeled cells were resuspended in BPB up to a volume of 1 ml, and 0.2-1 ml of blood solution was injected into the intravenous line to achieve the desired *in vivo* labeled cell density. For data

presented in Chapter 3, fRBC:RBC ratios ranged from 0.1% to 1.8%. Higher ratios were used to measure velocity and flux in small vessels, and lower ratios were used to measure flux in large vessels. For data presented in Chapter 4, an fRBC density of ~0.9% was used for measuring flux in large vessels, and a density of ~1.2% was used for measuring flux in capillaries.

Vessel diameter and RBC flux measurements

Fluorescein isothiocyanate (FITC) dextran (2000 kDa; 1 ml of 3% solution; Sigma FD200S) was administered intravenously to visualize the vasculature. Vessel lumenal diameter and RBC flux were measured simultaneously using confocal line scans oriented perpendicular to the vessel (Fig. 3.1, yellow line, Fig. 4.1). FITC and fRBCs were imaged using 488 and 635 nm laser lines, respectively. The confocal laser illumination was maintained as low as possible to minimize photoreceptor stimulation. Control experiments demonstrated that the confocal illumination did not reduce flicker-evoked vascular responses or retinal ganglion cell activity measured with extracellular electrodes. Two trial and stimulus paradigms were used for data acquisition. In the first, used for all blood vessels, the line-scan acquisition (~650 Hz) was at least 47 s in duration. However, this scan rate was too low to capture the passage of fRBCs in large arterioles and venules. To measure RBC flux in these vessels, additional data were gathered using ultrafast line scans (4200 Hz), in which the trial duration was limited to 8 s due to constraints of the confocal microscope software. Room illumination was dim during experimentation (~3 lux at the surface of the eye). For ease of processing and comparison, data were converted to a temporal resolution of 10 ms. All data were reviewed visually, and trials with eye movement or stimulus artifacts were excluded from additional processing.

Vessel diameter was calculated using a custom MATLAB (version R2012a; MathWorks) program that automatically extracted the borders of the vessel lumen from line-scan images (Fig. 3.1, Fig. 4.1*B1*). Light stimulus artifacts in line-scan images were automatically removed before diameter calculation, as were regions of the image in which the vessel was not significantly brighter than the background. The latter procedure

was particularly important in capillaries in which a single RBC passing through the vessel prevented visualization and measurement of the vessel lumen. Before analysis, vessel diameter data were temporally averaged using a symmetrical 1 s moving average filter. In many blood vessels, we observed a slow, steady decrease in diameter throughout the trial. This linear drift was removed from all diameter records in Chapter 4.

RBC flux was measured by two methods. In the first, unlabeled RBCs moving single-file in narrow vessels were visualized as dark bands interrupting the fluorescently labeled blood plasma (Fig 3.1C, Fig. 4.1*B1*). In the second method, fRBCs in vessels of all diameters were visualized as bright lines (Fig. 3.1B, Fig. 4.1*B3*). Using these two methods allowed us to calculate flux in all retinal vessels. In both methods, flux was calculated using a custom MATLAB program. RBCs were identified from the background using a moving thresholding algorithm. Line-scan lines that were darker (for true flux) or brighter (for fRBC flux) than surrounding lines were flagged as containing an RBC. A single RBC typically appeared on more than two adjacent line-scan lines. Adjacent RBC-containing lines were grouped together and considered a single RBC. Flux was calculated as RBCs per second.

In Chapter 4, measurement of vessel diameter and flux at a specific location on a blood vessel was made between two and eight times, and these trials were averaged to create a mean, which we call a series. All analyses presented in Chapter 4 are performed on series data, and this chapter's dataset contains 204 series from 47 rats.

Velocity measurements

Blood velocity was measured with line scans oriented either parallel (Fig. 3.1A, red line) or at a diagonal (Fig. 3.1A, blue line) to the blood vessel. 4,200 Hz line scans were used to capture fRBCs moving through vessels. In velocity line scan images (Fig. 3.1D,E) fRBCs appear as diagonal streaks where the angle of the streak is inversely proportional to velocity. Identification of streak angle was performed using the Radon function. Open source code for velocity calculation by (Chhatbar and Kara, 2013) was modified to fit the current dataset. All velocity line scans were processed by computing the velocity in bins of 500 rows (time axis), sliding 25 rows with each calculation. For

diagonal line scan data, 10 columns (vessel diameter axis) of 50 pixels each were used to calculate velocity across the width of the vessel. Vessel diameter was calculated from reference images of the FITC-filled vessel lumen. Due to chromatic aberration of the rat lens, the 488 and 635 images did not align perfectly. For this reason, all data are presented aligned to the furthest edges of the vessel that yielded usable velocity data.

Functional challenge

In Chapter 3, hyperoxia was generated by increasing the oxygen content of the ventilation gas from 30 to 60% and reducing nitrogen accordingly. Hypercapnia was generated by replacing 5% of the nitrogen with 5% CO_2. Both blood flow and blood vessel diameter were measured in primary arterioles every ~ 30 s during the challenge sessions, which typically lasted a total of ~13 min. Baseline diameter and flow values were collected for at least 2 min prior to challenge onset. Hyperoxia and hypercapnia were maintained for at least 3 min, after which inhalation gas mixtures were returned to normal and flow and diameter recovery was tracked.

In Chapter 4, the retina was stimulated with a 5 Hz diffuse flickering white light with a 10% duty cycle, an intensity of ~200 klux, and a duration of 15 s for long trials and 2 s for short trials. The stimulus light was long-pass filtered at 600 nm and directed obliquely onto the eye, illuminating the retina primarily through the sclera. Such a flickering stimulus effectively activates neurons of the inner retina (Miller, 2001).

Response onset time

Response onset time of a vessel was defined as the time to 20% of the peak diameter response. The peak response was calculated as the largest diameter within the first 4 s after stimulus onset, a procedure designed to isolate the first phase of the dilatory response (Fig. 4.3*A* shows a biphasic dilation in arterioles). The 20% onset time was measured only for those series in which the peak response within 4 s of stimulus onset was >3 SDs above the baseline. Onset time was not calculated for capillaries in the intermediate and deep capillary layers because these vessels lacked a clearly defined peak

during the first 4 s of the stimulus.

Immunohistochemistry

In Chapter 4 experiments, immediately after the animals were killed, the right (experimental) retina was prepared using an established whole mount protocol (Chan-Ling, 1997). After fixation (4% paraformaldehyde for 1 h) and blocking (10% donkey serum and 1% Triton X-100 in PBS for 4-12 h), retinas were incubated for 3 d with primary antibodies for rabbit-NG2 (1:1000; Millipore AB5320) and mouse-α-smooth muscle actin (α-SMA; 1:800; Dako M0851). Retinas were then washed and incubated for 2 d with the secondary antibodies donkey anti-rabbit-488 and donkey anti-mouse-594 (both 1:750 and from Jackson ImmunoResearch) and the blood vessel marker Isolectin GS-IB4-647 (1:75; Invitrogen I32450). Retinas were mounted on slides and imaged with confocal microscopy. The area of the retinal whole mount that matched the area we measured *in vivo* was imaged to determine vessel branch order, the strength of α-SMA expression, and the distance of each *in vivo* measurement location to the nearest pericyte soma. The distinctive pattern of vessel branching facilitated matching the *in vivo* and whole-mount retinal areas (see Fig. 4.7*A*).

We measured α-SMA expression by assigning each measured vessel segment an α-SMA expression level of low, medium, or high. This assignment was based on the intensity of α-SMA staining relative to the rest of the vascular tree and the intensity of the fluorophores that labeled NG2 and isolectin. To reveal α-SMA expression in first-order arterioles, antibody penetrance was increased by enzymatically digesting the retinas with collagenase/dispase (2 mg/ml in PBS for 30 min; Roche 269 638) before blocking.

Calculation of fRBC:RBC ratio and measurement of hematocrit

In Chapter 3 experiments, the fRBC:RBC ratio was calculated using both in vivo flow cytometry and a slide-based cell counting method. To calculate the fRBC:RBC ratio using in vivo flow cytometry, total RBC flux and fRBC flux were simultaneously acquired with perpendicular line scans across capillaries, where blood cells move single-

file (Fig. 3.1C, Fig. 4.1C). Labeled and total cells/s were counted and their ratio calculated.

The fRBC:RBC ratio and number of cells per blood volume were also calculated using a hemocytometer (Hausser Scientific, 3102). Blood withdrawn from the rat at the end of each experiment in Chapter 3 was diluted 1:300 with BPB and loaded onto an unlined two-chamber hemocytometer. An upright fluorescence microscope with a 20X water-immersion objective was used to visualize labeled and unlabeled cells. 10-20 fields were imaged in each of the two chambers of the hemocytometer. FITC and 635 nm fluorescence cubes were used to visualize all RBCs and fRBCs, respectively. Using a custom MATLAB algorithm, these images were intensity rescaled, median filtered, and background subtracted. The circular RBCs in each channel were identified and counted. Because each imaged field of the hemocytometer represents a defined volume, these cell counts were used to calculate the number of cells per volume as well as the fRBC:RBC ratio. Values from the two chambers did not differ, so the data were pooled.

Vessel density

Vessel density in the three vascular layers was quantified in five immunohistochemically labeled retinas in regions near *in vivo* imaged areas that did not contain large arterioles or venules. Vascular layers were easily distinguished from one another by their retinal depth and unique vessel morphologies. Confocal *z*-stacks of NG2, α-SMA, and isolectin labeling were acquired for each layer. Z-stacks were summed and further processed using NIH ImageJ (version 1.46r) to isolate blood vessels from the background. Vessels were skeletonized, and the total blood vessel length in each vascular layer was calculated using the Montpellier ROI ImageJ macro (http://www.mri.cnrs.fr/index.php?m=67&&l=2).

Statistical methods

For all analyses, significance was defined as $p < 0.05$. Statistical analysis was performed using GraphPad Prism (version 5) and MATLAB.

Chapter 3: Data are expressed as mean ± standard deviation. A Pearson linear correlation was used to quantify correlations between blood flow measurements calculated two ways. Two-tailed t-tests were used to test for differences between parent and daughter vessels in the bifurcation data. Repeated measures ANOVAs were used to assess changes in diameter and flow in response to hyperoxic and hypercapnic challenge.

Chapter 4: Data are expressed as mean ± SEM, with *n* representing the number of series unless otherwise noted. *P* values for group comparisons are from ANOVA with *post hoc* Bonferroni's tests for parametric data and from Kruskal–Wallis tests with *post hoc* Dunn's tests for nonparametric data. A repeated-measures ANOVA was performed to identify differences in capillary layer density (Fig. 4.2*C*). Least-squares linear regression was performed to test for an effect of pericyte distance on capillary dilation (see Fig. 4.6*B*). Because of a high degree of skew, onset time data are reported as median ± median absolute deviation and presented in Fig. 4.4*D* as box plots.

Chapter 3: Precise measurement of blood flow in retinal vessels with labeled red blood cells

Summary

Measuring blood flow in the retina is challenging in part due to the wide range of vessel sizes present. Most existing optical techniques for measuring blood flow are limited to large vessels and require expensive equipment and complex computation. We have characterized a direct and inexpensive method of measuring absolute blood flow in vessels of all sizes in the rat retina. This method uses ultra-fast confocal line scans to track the passage of fluorescently labeled red blood cells (fRBCs). The ability of this method to determine blood flow was verified a number of different ways including by measuring total retinal blood flow, and looking at changes in blood flow following hyperoxic and hypercapnic challenge. Confocal line scans parallel or perpendicular to the vessel were also used to compute the velocity of fRBCs moving through the vessel. We have demonstrated that this method provides accurate measures of absolute blood flow and velocity in all rat retinal vessels, making it a good option for research groups looking for an easy and direct way to measure parameters of blood flow.

Introduction

Blood flow is closely tied to the metabolic state of the central nervous system (CNS) under physiological and pathological conditions. Blood flow is disrupted in many CNS disorders, and retinal blood flow disruption can cause severe vision loss. Reductions in blood flow and blood vessel reactivity occur in early stages of diseases such as Alzheimer's disease, diabetic retinopathy, and glaucoma. Precise measurements of retinal blood flow in humans and in animals models can be used to track disease onset and progression and inform treatment.

Many different methods have been developed for measuring blood flow (Pournaras and Riva, 2013). Estimates of blood flow can be made by counting large (~15 μm) microspheres that lodge in capillaries (Ahmed et al., 2001), measuring transit time of labeled plasma, and measuring oxygenation with functional magnetic resonance imaging (Cheng et al., 2006; La Garza et al., 2010) or phosphorescence lifetime imaging (Shahidi et al., 2006, 2009; Wanek et al., 2011). More commonly, blood flow is computed as the product of blood velocity and vessel cross-sectional area, each measured independently. Vessel diameter is measured from fundus images, using the Retinal Vessel Analyzer, scanning laser ophthalmoscope, or confocal line scans, while velocity can be measured with bidirectional laser Doppler velocimetry, frequency domain optical coherence tomography (FD-OCT), video analysis of fluorescently labeled red blood cells (fRBCs) or small microspheres (Lorentz et al., 2008; Rovainen et al., 1993), or line scan analysis of RBC streaks (Autio et al., 2011; Hutchinson et al., 2006; Kim et al., 2012; Kleinfeld et al., 1998; Santisakultarm et al., 2012; Schaffer et al., 2006).

Non-invasive optical techniques of measuring retinal blood have gained favor due to their applicability in human subjects. Recent technological advancements include the Canon laser Doppler blood flowmeter, a commercially available instrument that uses Doppler velocimetry and diameter measurements to calculate blood flow (Garcia et al., 2002; Gilmore et al., 2005; Guan et al., 2003; Sehi et al., 2012). FD-OCT, which computes blood flow by integrating velocity across the vessel cross-section (Doblhoff-Dier et al., 2014; Shahidi et al., 2014; Wang et al., 2007, 2009), reviewed by Leitgeb et al (2014), is also used. However, the major drawback of most optical methods is that blood flow measurements are limited to vessels greater than ~30 μm in diameter; smaller vessels require higher resolution techniques.

To this end, we have characterized a set of techniques for precisely measuring blood flow in the retinal vessels of the rat, which range from ~4 to ~70 μm in diameter. We measure blood flow by visualizing the passage of fRBCs. This technique is relatively non-invasive, requiring only withdrawal and re-injection of blood. Our measurements are direct. Minimal computation and few assumptions are needed to calculate flow. Imaging of fRBCs has been used previously to measure blood flow in small vessels where blood

velocity is low enough that the passage of individual cells can be easily imaged. We use ultra-fast confocal line scans to capture the passage of individual fRBCs in retinal blood vessels of all sizes and are not limited to low-velocity vessels. We have used this technique to precisely measure total blood flow in the retina, blood flow changes in response to functional challenge, and blood velocity profiles across the width of vessels. Absolute blood flow can be measured easily and accurately with this technique.

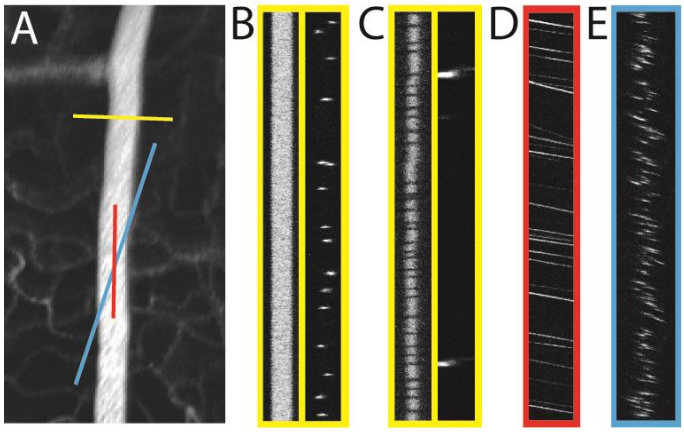

Figure 3.1: Line scans can measure multiple blood flow parameters. ***A***, A confocal reference image showing three line scan configurations for measuring flux and diameter (yellow) and velocity (red and blue). ***B***, In large vessels, lines oriented perpendicular to the vessels yield diameter (left) and fRBC flux (right) data. ***C***, In very small vessels, perpendicular line scans allow for simultaneous measurement of diameter and total RBC flux (left) and fRBC flux (right). ***D***, Line scans parallel to the vessel wall provide measurements of velocity. Velocity is inversely proportional to the angle of the fRBC streaks. ***E***, Line scans oriented diagonally across the vessel yield fRBC streaks where angles vary across the vessel's width.

Results

We have measured blood flow in rat retinal blood vessels by introducing fluorescently labeled red blood cells into the vasculature (Fig. 3.1). fRBC flux was measured with perpendicularly oriented confocal line scans in vessels ranging from primary arterioles and venules to capillaries by counting individual fRBC as they passed through a vessel (Fig. 3.1A, yellow line, and B, C). In small vessels where cells move single file, fRBC and total RBC flux can be captured simultaneously (Fig. 3.1C).

Velocity was measured at a single location within a vessel with confocal line scan lines oriented parallel to the lumen (Fig. 3.1A, red line, and D). Velocity was also measured across the full width of blood vessels with diagonally oriented line scan lines (Fig. 3.1A, blue line, and E).

fRBC:RBC ratio and hematocrit measured in vivo and in vitro

Our methodology allows us to measure absolute blood flow, expressed as µL/min, with high accuracy. Blood flow measurements obtained by counting fRBCs require knowledge of the fRBC flux, the fRBC:RBC ratio and the number of RBCs per volume of blood. The fRBC:RBC ratio can be measured both by in vivo flow cytometry and by in vitro cell counting using a hemocytometer. The fRBC:RBC ratios measured by in vivo flow cytometry, obtained by simultaneously counting the fRBCs and unlabeled RBC passing through a capillary (Fig. 3.1C), equaled the ratios measured using a hemocytometer in three of four experiments where both measurements were made (in vivo vs in vitro, 1.64 ± 0.35%, n = 8 vs 1.52 ± 0.35%, n = 9, 1.50 ± 0.42%, n = 9 vs 1.52 ± 0.60%, n = 16, 0.69 ± 0.24%, n = 9 vs 0.71 ± 0.35%, n = 32, n.s.; 0.53 ± 0.36%, n = 8 vs 0.22 ± 0.22% n = 36, $p < 0.01$; two-tailed t-tests). fRBC:RBC ratios ranged from 0.1% to 1.8%, and we note that the experiment where in vivo and in vitro values were not statistically equal was one with a very low fRBC:RBC ratio.

RBCs/µL was calculated for each experiment by counting the total number of RBCs in the hemocytometer imaging fields that have a known volume. In our experiments, the mean number of RBCs/µL was 9.6 ± 1.1 million, fitting well within the accepted range of 7-10 million RBCs/µL.

Blood flow calculated from RBC flux and velocity

Blood flow (Q) was calculated by two independent methods that were then compared, allowing us to validate the techniques. In the first method, we used fRBC flux to compute blood flow using the equation Q = (fRBCs/s)*(RBCs/fRBCs)/(RBCs/vol), where RBCs/vol was determined from hemocytometer measurements. In the second method, RBC velocity and vessel diameter were measured using confocal line scans

parallel and perpendicular to blood vessels. Blood flow was calculated from the equation Q = V*A, where V is velocity and A is the luminal cross-sectional area. V was measured from luminal line scans in the middle of blood vessels. As discussed below, this yielded velocities that approximated the average RBC velocity within the vessel.

Blood flow was calculated by these two methods in vessels with a range of diameters and flow rates. The two methods yielded blood flow values that were highly correlated (Fig. 3.2; $R^2 = 0.982$; $p < 0.001$; Pearson linear correlation) with a slope deviating from unity by 0.13. Because fRBC flux, blood velocity, blood vessel diameter, and blood cell counts are all measured independently, the highly correlative relationship between the flow values confirms the validity of the methods.

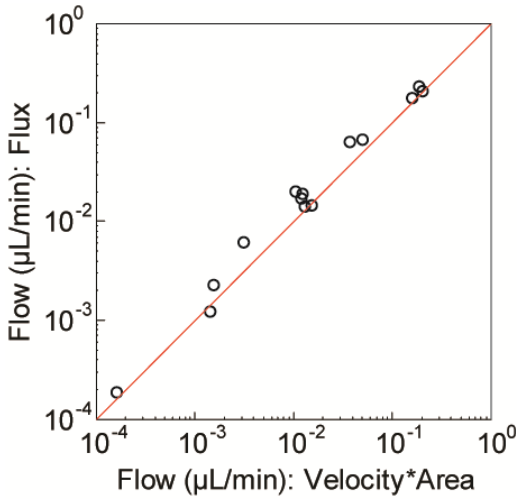

Figure 3.2: Flow values calculated using two independent methods are comparable. Blood flow was calculated two ways and the two methods are plotted against each other. The x axis computation used diameter and velocity data and the y axis computation use fRBC flux data. Axes are on the log scale. The red line represents unity.

Blood flow at bifurcations

We measured fRBC flux in parent and daughter vessels at bifurcations (Fig. 3.3A) to further validate our blood flow measurement technique. The sum of the RBC flux in the two daughter vessels should equal the flux in the parent vessel. This technique has been used previously to validate blood flux measurements (Parthasarathi et al., 1999). For

all bifurcations studied, the sum of the fluxes in the daughter vessels was nearly identical to that of the parent vessel (Fig. 3.3B). This was true for vessels across a range of fluxes. The parent and daughter fluxes were highly correlated (Fig. 3.3B, $R^2 = 0.995$, $p < 0.001$; Pearson linear correlation) with a slope deviating from unity by 0.12. The ratio of the flux in the parent vessel to the fluxes in the two daughter branches was 0.89 (Fig. 3.3C; n = 6). Parent vessels averaged 9.3 ± 3.5 μm and daughter vessels 8.4 ± 2.9 μm in diameter. The ratio of the diameter of the parent vessel to the sum of the diameters of the daughter vessels was 0.54 (Fig. 3.3C).

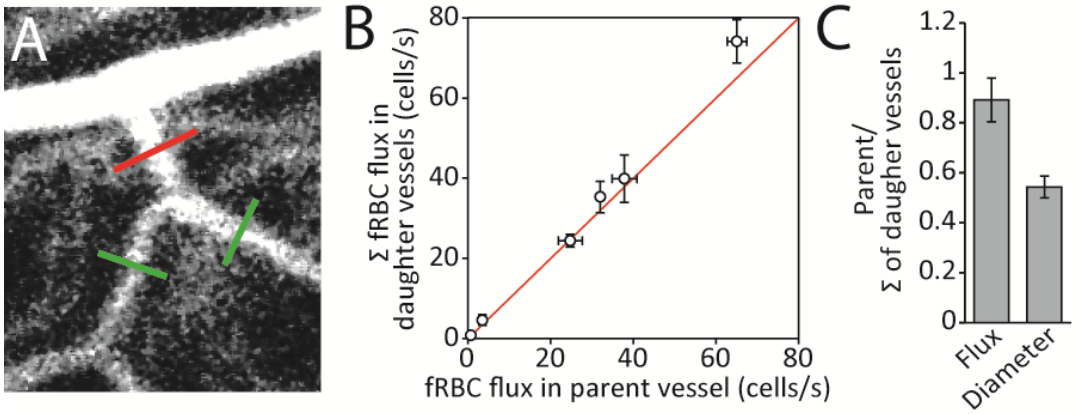

Figure 3.3. Flux and diameter at bifurcations. ***A***, Confocal reference image showing a typical bifurcation. The red line represents line scans performed across the parent vessel, the green lines represent line scans performed across the two daughter vessels. ***B***, The mean flux for the parent vessel is plotted against the sum of flux in the daughter vessels for the six bifurcation points sampled. The red line represents unity. ***C***, The ratio of the parent to sum of daughter vessels was calculated for flux and diameter.

Total retinal blood flow

Total retinal blood flow was measured by summing the flow in all primary arterioles or venules emerging from the optic disk. Flow in these primary vessels was predictably dependent upon their diameter and type (Fig. 3.4A). The average flow in individual primary retinal arterioles and venules was 0.42 ± 0.25 and 0.40 ± 0.25 μL/min. The average diameter of the arterioles and venules was 30.0 ± 6.7 and 46.5 ± 16.5 μm (n = 4 retinas, 32 arterioles and 29 venules). The ratio of the number of arterioles to venules

in this sample was 1.10. The relationship between flow and diameter can be described roughly by power functions with exponents of 2.30 (R^2 = 0.65) and 2.23 (R^2 = 0.79) for arterioles and venules, respectively. These values are similar to the exponents of 2.76 and 2.84 reported previously (Riva et al., 1985).

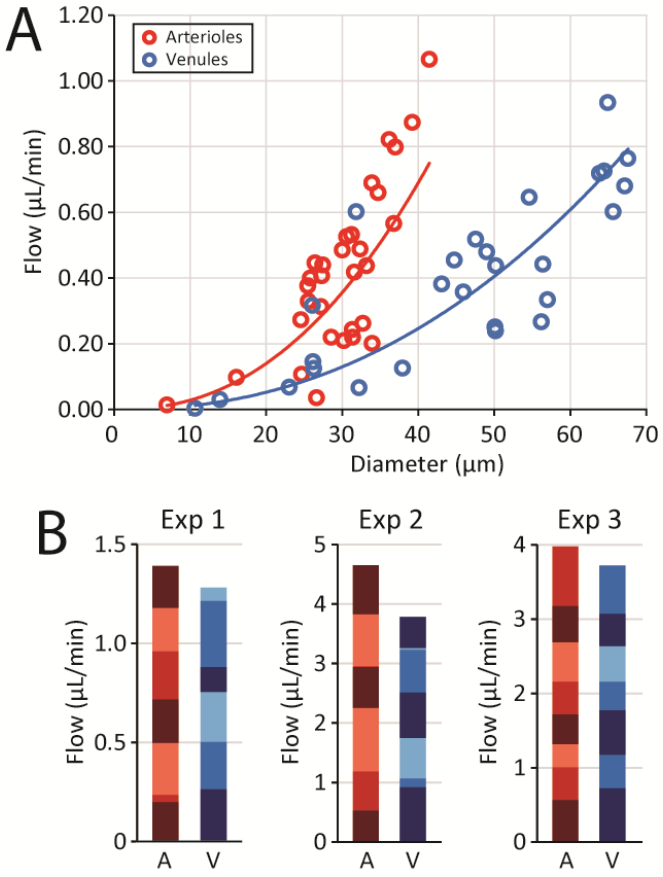

Figure 3.4. Total retinal blood flow. ***A***, Blood flow in individual arterioles (red) and venules (blue) emerging from the optic disk are plotted by diameter and fit with power functions. ***B***, Total blood flow in retinas from 3 experiments. Left columns represent arterioles (A) and right columns represent venules (V). Each color block indicates the flow in an individual blood vessel. Total bar height is the sum of individual flows for each vessel type, which corresponds to the total blood flow in arterioles or venules for each retina.

Because all blood that enters the retina through arterioles must leave it through venules, we expected that total blood flow in arterioles would equal the total blood flow in venules. To calculate the total blood flow in arterioles or venules, we summed the

individual flows of all vessels of that type in the retina. We found that total blood flow in arterioles was consistently higher than in venules. Arteriole flow averaged 3.34 µL/min while venule flow averaged 2.93 µL/min. The ratio of arteriole:venule blood flow was 1.13 for the three retinas examined (Fig. 3.4B). The reason for this discrepancy is unclear.

Total retinal blood flow, calculated as the average of arteriole and venule flows, was 1.34, 4.22, and 3.85 µL/min for the three retinas examined, with a mean of 3.14 µL/min. The large variation in total blood flow between retinas is not unexpected, as blood flow in human retinas is also variable (Garhofer et al., 2012; Tayyari et al., 2014).

Functional challenge

We challenged animals with hyperoxia and hypercapnia, two stimuli known to affect retinal blood flow, to confirm that our measurements are sensitive to changes in blood flow on a short timescale.

Hyperoxia, generated by raising inhaled O_2 from 30 to 60%, constricted vessels and decreased blood flow (Fig. 3.5A). Arteriole constrictions averaged 6.4 ± 2.3%, a significant reduction from baseline diameters ($p < 0.01$; repeated-measures ANOVA; $n = 4$), and blood flow decreased by an average of 15 ± 3.8% from baseline (Fig. 3.5B; $p < 0.05$). Following the return to normoxia, diameter and flux shifted toward baseline, although only diameter was indistinguishable from baseline. The changes in diameter and blood flow had a slow onset and offset, taking approximately 1 minute to reach steady states.

Hypercapnia, generated by breathing 5% CO_2, triggered a dilation of 59.7 ± 12.1% and a blood flow increase of 115.2 ± 17.0% (Fig. 3.5C and D) that were statistically higher than baseline levels ($p < 0.001$ and $p < 0.01$, respectively; $n = 3$). The blood flow changes were faster than for hyperoxia, taking approximately 30 seconds to peak and return to baseline. Diameter and flow values after hypoxia ended were indistinguishable from baseline values.

The changes we observed in blood flow matched published values (Sehi et al., 2012). Although blood flow changes were larger than diameter changes for both

hyperoxia and hypercapnia, the fourth-power relationship predicted by the Poiseuille equation was not borne out.

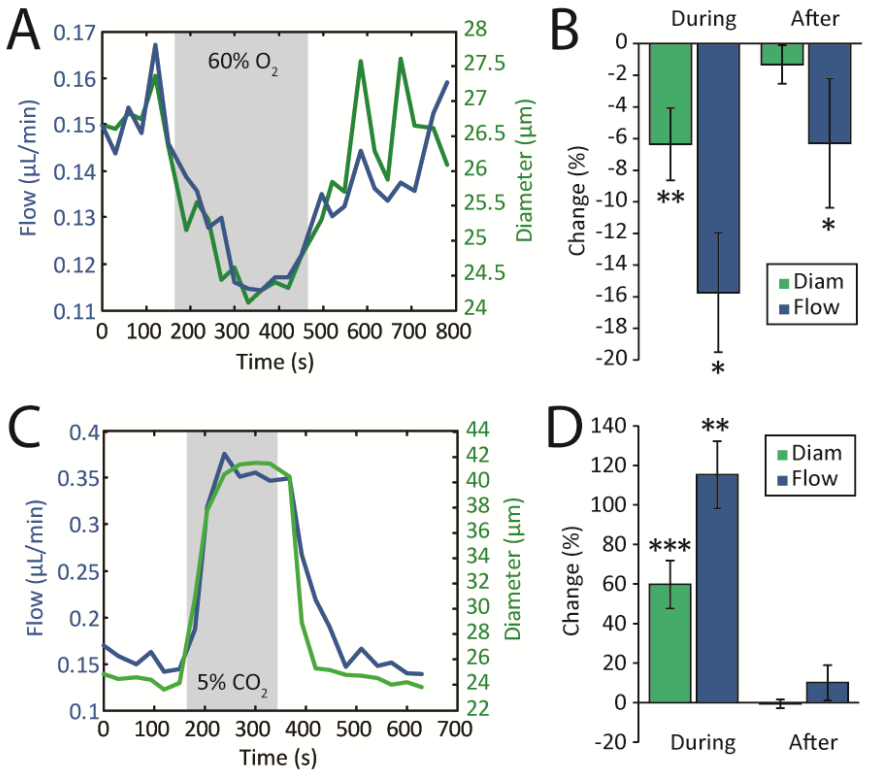

Figure 3.5. Blood flow changes in response to hyperoxic and hypercapnic challenge. Representative traces of flow (blue) and diameter (green) in response to hyperoxia (***A***) and hypercapnia (***C***). Gray background indicates the presence of hyperoxic or hypercapnic gas mixture. ***B & D***, Percent change in diameter and flow during and after the change in blood gas are summarized in bar graphs. *p < 0.05, **p < 0.01, ***p < 0.001.

Velocity profile across the width of vessels

In theory, blood velocity in rigid, straight, non-branching vessels containing a homogenous fluid should follow a parabolic relation across the width of the vessel, with velocity maximal at the vessel center and approaching zero at the edges. However, a perfect parabolic relation does not typically occur in blood vessels in vivo. We used two different approaches to measure velocity profiles of large retinal arterioles and venules.

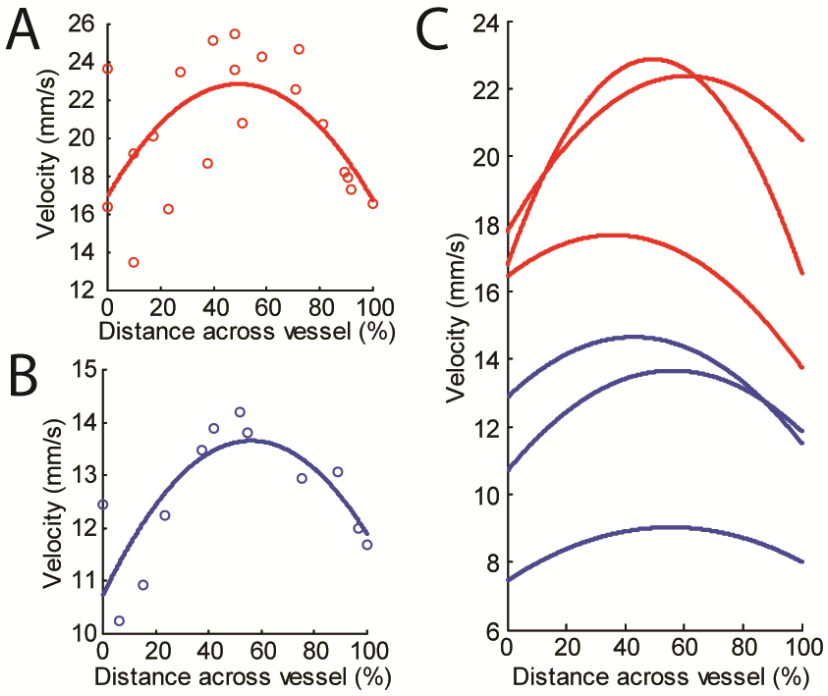

Figure 3.6. Velocity across the profile of blood vessels using parallel line scans. ***A & B***, Using parallel line scans, velocity was determined at many points across the profile an arteriole (***A***) and a venule (***B***) and these velocity measurements were fit with a two-degree polynomial (solid lines). ***C***, Fits are shown for all the arterioles (red) and venules (blue) studied.

Parallel line scans. High frequency line scans parallel to the vessel were acquired at multiple locations across the vessel's width. These line scan images yield slanted lines created by fRBCs as they move through the vessel (Fig. 3.1D). Shallower angles indicate higher velocity. For each line scan trial, the average fRBC velocity was plotted as a function of the position within the blood vessel. Each vessel's dataset was fit with a quadratic equation. Raw data and the parabolic fit for a representative arteriole and venule are shown in Figs. 3.6A and B. As expected, velocities were lowest at the vessel edges and highest in the vessel's center (Fig. 3.6C). The mean maximum velocities were 21.0 mm/s for arterioles with an average diameter of 28.4 μm, and 12.4 mm/s for venules with an average diameter of 35.7 μm.

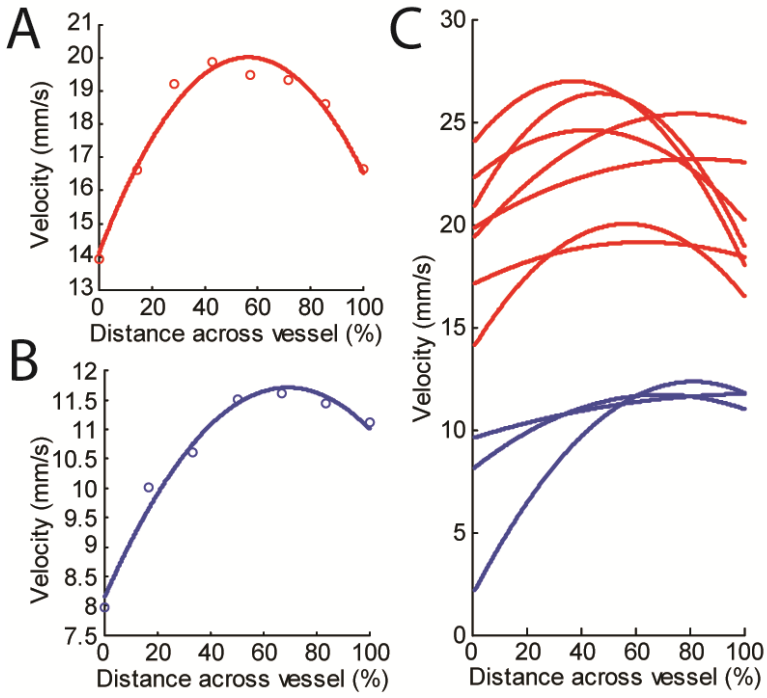

Figure 3.7. Velocity across the profile of blood vessels using diagonal line scans. ***A & B***, Velocities calculated across the profile of an arteriole (***A***) and venule (***B***). Individual velocity measurements are fit with a two-factor polynomial (solid lines). ***C***, Parabolic fits for all arterioles (red) and venules (blue) studied.

Diagonal line scans. We used a second method to measure velocity profiles in single trials. High frequency line scans oriented diagonally across a vessel (Fig. 3.1E) were used to measure the velocity of individual fRBCs at different positions across the vessel width. Velocity was computed at 10 positions along the line. The advantage of this method is that the full velocity profile can be determined from a single line scan. Examples of velocity profiles from an arteriole and venule are shown in Fig. 3.7A and B. Fitting the data from each trial with a quadratic equation yielded an average maximum velocity of 23.7 mm/s for arterioles and 11.9 mm/s for venules (Fig. 3.7C).

Although we did not measure velocity profiles in a comprehensive sample of arterioles and venules, the velocity values and parabolic shapes of the profiles were similar between those obtained with parallel and diagonal line scans.

Discussion

We have characterized a technique that can precisely measure blood flow in rat retinal vessels. By capturing the passage of individual fRBCs through vessels, and by using a simple method of correcting fRBC flux to account for the fRBC/RBC fraction and RBCs per volume, absolute blood flow was measured with high precision and temporal resolution in vessels ranging from 4 to 70 μm in diameter. We validated the accuracy of our measurements a number of different ways. First, we compared our blood flow measurements to a second independent method of calculating blood flow that is based on fRBC velocity and vessel diameter. Second, we ensured that blood flow in parent and daughter vessels at bifurcations matched expected values. Third, we observed expected blood flow changes following hypercapnic and hyperoxic challenges. Finally, we observed parabolic velocity profiles in blood vessels as small as 20 μm in diameter.

Blood flow at bifurcations

The validity of our method was tested at vessel bifurcations, where the sum of blood flow in daughter branches is equal to flow in the parent vessel. Conservation of blood flow was indeed observed, providing assurance that our method accurately captured the passage of individual RBCs in different caliber vessels. Murray's law predicts the vessel radii required for maximum energetic efficiency of a branching system. Theoretically, the radii of parent (r_p) and daughter (r_{d1} and r_{d2}) vessels follows a power law, where $r_p^k=r_{d1}^k+r_{d2}^k$ and the exponent k ranges from 2 to 3. This was not observed in our bifurcation dataset, where k averaged 6.8. A study of the cerebral vasculature shows a wide variability of k values (Cassot et al., 2009), with the current result close to their reported mean of 6.2. Our results confirm previous findings that Murray's law does not accurately model vascular bifurcations, particularly in microvessels (Cassot et al., 2009; Hirsch et al., 2012).

Total retinal blood flow

We have used fRBC flux measurements to calculate total blood flow in the retinal vasculature. Total blood flow was measured as the sum of flow in all individual primary

arterioles or venules in a retina. Our blood flow estimate of 3.14 µL/min is on the low end of published values for the rat retina, which range from 2.1 µL/min using fRBCs (Khoobehi et al., 2003) to 16 µL/min using microsphere tracking (Leskova et al., 2013). Anesthetic also has a strong effect on blood flow; a study using OCT found blood flow was 3.3 µL/min under ketamine/xylazine and 6.4uL/min under isoflurane/xylazine (Choi et al., 2012). We observed a wide variability of total flow between individual rats, which is expected based on published work. We note a consistent blood flow underestimation of 12.2% in venules compared with arterioles, the cause of which is unclear.

Comparison to other methods of measuring blood flow

Variations of the fRBC imaging method have been applied for the past 30 years (Collins et al., 1998; Kornfield and Newman, 2014; Sarelius and Duling, 1982; Schulte et al., 2003; Unthank et al., 1993; Wright and Harris, 2008; Zimmerhackl et al., 1983). fRBC imaging has been used to measure capillary flux and velocity by tracking the movement of labeled cells in video frames (Ben-nun, 1996; Ben-nun et al., 1992; Hudetz et al., 1995; Krolo and Hudetz, 2000; Parthasarathi et al., 1999; Reyes-Aldasoro et al., 2008; Schulte et al., 2003; Seylaz et al., 1999; Wang et al., 2011; Wright and Harris, 2008; Yamaguchi et al., 1992), using confocal microscopy (Pinard et al., 2002; Tomita et al., 2011; Villringer et al., 1994), and using scanning laser ophthalmoscopy (Wajer et al., 2000). Sophisticated scanning techniques have also been applied to generate 3D maps of velocity and flux in normal and tumorous brain tissue (Kamoun et al., 2010). In the current study we have used fRBC imaging to measure blood flow in large vessels as well as capillaries, a method that affords significant insights into blood flow dynamics in the retina.

Our method of measuring absolute blood flow has distinct advantages over other methods. Measurements based on bidirectional laser Doppler velocimetry, the retinal vessel analyzer, and OCT are limited to vessels larger than 30 µm in diameter and are at their most accurate in large diameter vessels. Conversely, our technique can be used to measure flow in all rat retinal vessels. Unlike optical methods of measuring blood flow, which require sophisticated computations to extract flow values and are subject to

interference, our technique is extremely straightforward. It is based on simple cell counts, which we have shown to be reliable and accurate. Further, it is relatively inexpensive compared to instruments such as the retinal vessel analyzer and OCT setups. It requires only a confocal microscope and the dye solutions to label RBCs.

The primary limitation of this method is that it requires confocal line scans, which can only be done on one vessel at a time if high temporal resolution is to be preserved. Because the technique involves blood draws and re-injection, it is unlikely to be favored for human subjects over less invasive, though also less direct, techniques for blood flow measurement. However, the technique is particularly useful in animal studies, where flow can be measured in all vessels regardless of size and invasiveness is not an issue.

Parabolic velocity profiles

We measured the velocity of fRBCs using confocal line scans to determine velocity profiles across the width of primary arterioles and venules. The profiles in vessels between 20 and 50 μm in diameter were roughly parabolic. The two methods we used to capture the velocity profiles, parallel and diagonal line scans, yielded similar data. Since diagonal line scans require only a single trial to capture the entire profile and are therefore not subject to inter-trial shifts in velocity, they may be preferable to parallel scans. The advantages and limitations of these two methods have been discussed previously (Kamoun et al., 2010). The maximum velocities for arterioles and venules match published values well (Doblhoff-Dier et al., 2014), although they are below velocities measured using fluorescent microspheres (Lorentz et al., 2008).

The parabolic velocity profiles we obtained resemble values reported for larger vessels but do not perfectly match theoretical estimates. There are a number of reasons for this. First, we cannot capture the true maximum fRBC velocity due to our imaging system's relatively large depth of field. Velocity measurements in the center of a vessel in the x-y plane will include velocity values from RBCs at the vessel's edges in the z plane. Therefore, our estimates of maximum velocity are underestimated and approximate the average fRBC velocity. This velocity underestimation will cause the parabolic blood velocity profiles to be blunted at their apex, an observation reported

previously (Logean, Eric and Schmetterer, 2003; Parthasarathi et al., 1999; Rovainen et al., 1993; Zhong et al., 2011). Second, although some studies detect zero velocity at vessel edges using Doppler-based systems (Yazdanfar et al., 2003; Zhi et al., 2011), we did not. This is not surprising for vessels in the diameter range of 20-50 μm, where the width of a single RBC represents a significant fraction of vessel's diameter. As vessel diameter decreases, individual RBCs take up a proportionally larger area of the lumen and their interactions with each other and the vessel wall disrupt laminar flow (Zhong et al., 2011).

Conclusions

Our results demonstrate that blood flow can be measured accurately in vessels from 4 to 70 μm in diameter by imaging fRBCs with ultra-fast line scans. Flow estimates obtained from fRBC flux measurements match those calculated from RBC velocity and vessel diameter. Flow at vessel bifurcations confirm the accuracy of the technique. Measurements of total blood flow in the retina and velocity profiles across the width of vessels are easily obtained. The method will prove useful in future studies of blood flow and metabolism in the retina and throughout the CNS.

Chapter 4: Regulation of Blood Flow in the Retinal Trilaminar Vascular Network

Summary

Light stimulation evokes neuronal activity in the retina, resulting in the dilation of retinal blood vessels and increased blood flow. This response, named functional hyperemia, brings oxygen and nutrients to active neurons. However, it remains unclear which vessels mediate functional hyperemia. We have characterized blood flow regulation in the rat retina *in vivo* by measuring changes in retinal vessel diameter and red blood cell (RBC) flux evoked by a flickering light stimulus. We found that, in first and second-order arterioles, flicker evoked large (7.5 and 5.0%), rapid (0.73 and 0.70 s), and consistent dilations. Flicker-evoked dilations in capillaries were smaller (2.0%) and tended to have a slower onset (0.97 s), whereas dilations in venules were smaller (1.0%) and slower (1.06 s) still. The proximity of pericyte somata did not predict capillary dilation amplitude. Expression of the contractile protein α-smooth muscle actin was high in arterioles and low in capillaries. Unexpectedly, we found that blood flow in the three vascular layers was differentially regulated. Flicker stimulation evoked far larger dilations and RBC flux increases in the intermediate layer capillaries than in the superficial and deep layer capillaries (2.6 vs 0.9 and 0.7% dilation; 25.7 vs 0.8 and 11.3% RBC flux increase). These results indicate that functional hyperemia in the retina is driven primarily by active dilation of arterioles. The dilation of intermediate layer capillaries is likely mediated by active mechanisms as well. The physiological consequences of differential regulation in the three vascular layers are discussed.

Introduction

The brain has high metabolic requirements, consuming 20% of the energy of the body while constituting only 2% of its mass. Oxygen and glucose delivery to the brain is critical for maintaining proper function, and the mechanisms that regulate blood flow are

both complex and essential. On a global level, the blood supply of the brain is controlled by autoregulatory mechanisms that compensate for variations in blood pressure. On a fine spatial scale, functional hyperemia regulates blood flow in response to local neuronal activity. Increased synaptic activity results in the dilation of blood vessels, increased blood flow, and reduced blood deoxyhemoglobin. The latter response is exploited to generate functional brain images using the BOLD technique. Recent work has elucidated the neurovascular coupling mechanisms underlying functional hyperemia, a quest that has implicated both neurons and glial cells (Attwell et al., 2010). Despite the importance of functional hyperemia to brain function, it remains incompletely understood.

It is well known that arterioles regulate blood flow in the brain (Boas et al., 2008; Devor et al., 2007; Vanzetta et al., 2005). However, the role of capillaries in actively regulating blood flow remains uncertain. Active capillary dilation would deliver oxygen with much greater spatial precision than arterioles. An active capillary role is supported by work in olfactory glomeruli (Chaigneau et al., 2003) and the subventricular zone (Lacar et al., 2012). In addition, pericytes, contractile cells that surround capillaries, can regulate capillary diameter in both the retina and cortex (Hamilton et al., 2010; Peppiatt et al., 2006; Puro, 2007; Schönfelder et al., 1998), and pericytes in the somatosensory cortex dilate vessels in response to sensory stimulation (Hall et al., 2014). In contrast, another report indicates that capillaries respond passively and that active pericyte relaxation does not contribute to cortical functional hyperemia (Fernández-Klett et al., 2010).

We now address the questions of blood flow regulation and active control of blood flow by capillaries in the *in vivo* retina. The retina offers several advantages in studying functional hyperemia. It can be imaged non-invasively, its vasculature is easily visualized, it has a high density of capillary pericytes, and it can be stimulated physiologically with light. The retinal vasculature is a highly interconnected structure composed of three planar vascular layers at different retinal depths (Ganesan et al., 2010; Genevois et al., 2004; Ivanova et al., 2014; Paques et al., 2003; Stahl et al., 2010). To our knowledge, functional hyperemia in the three retinal vascular layers has not been described previously.

We have characterized blood flow regulation by measuring flicker-evoked changes in vessel diameter and red blood cell (RBC) flux in arterioles, capillaries, and venules in the rat retina. We find that flicker-evoked dilations are larger and faster in arterioles than in downstream capillaries and venules. Intriguingly, we find that functional hyperemia differs dramatically in the capillaries of the three vascular layers.

Results

The retinal vasculature is composed of three distinct vascular layers. The central retinal artery and vein branch at the optic disc to form arterioles and venules, which lie on the retinal surface adjacent to the vitreous humor. Branches of the arterioles make up the superficial vascular layer. We define these vessels by order. First-order arterioles branch directly off of the central retinal artery, and each subsequent branch has an incrementally higher order (Fig. 4.1*A*). We define first-, second-, and third-order vessels as arterioles and vessels of fourth order and greater as capillaries. The vast majority of capillaries in the superficial layer dive into the retina to form the intermediate vascular layer, a network of capillaries at the border of the inner nuclear and the inner plexiform layers. Capillaries in the intermediate layer traverse parallel to the retinal surface for only a short distance before they dive farther into the retina to form the deep vascular layer, which is a dense, interconnected meshwork of capillaries at the border of the inner nuclear and the outer plexiform layers. The deep layer capillaries connect to small draining venules, which rise back to the retinal surface and connect to large venules. Diving capillaries and draining venules were not characterized in this study. The connectivity of the trilaminar vascular network is schematized in Figure 4.2*A*. Morphological analysis suggests that 70% of the blood entering the retina initially flows through the superficial capillaries and then through the intermediate and deep layer capillaries before exiting the retina (Paques et al., 2003).

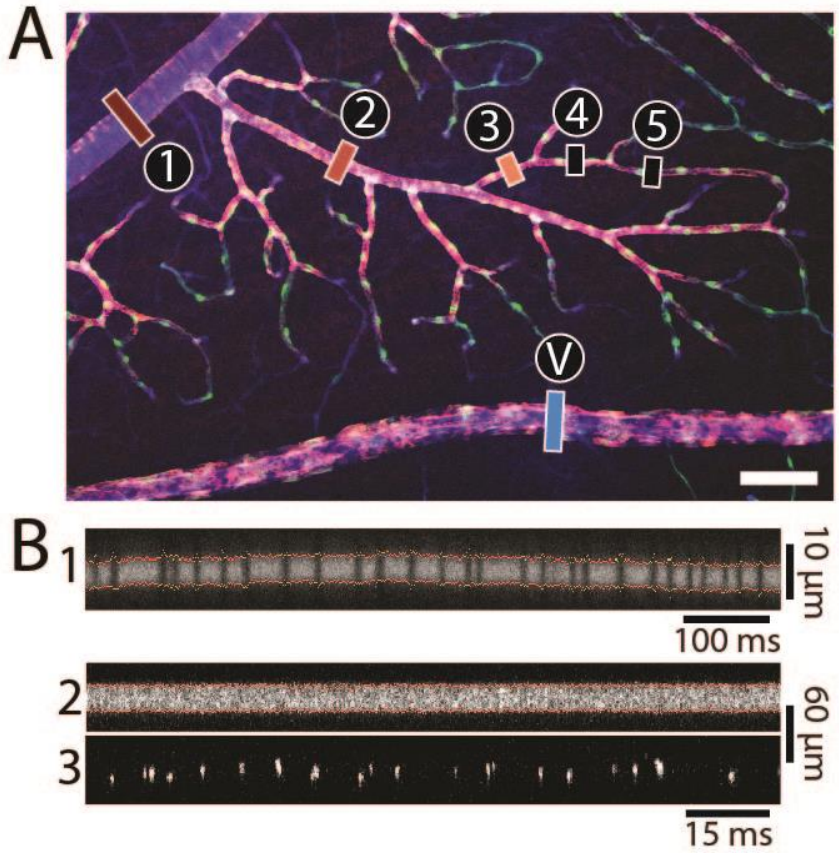

Figure 4.1. Measurement of blood vessel diameter and RBC flux in the retina. ***A***, Confocal image of a whole-mount retina labeled for the blood vessel marker isolectin (blue), the contractile protein α-SMA (red), and the pericyte marker NG2 (green). Blood vessel order in the superficial vascular layer is indicated. First-order arterioles (1) branch from the central retinal artery. Each subsequent branch (2-5) has a higher order. Venules (V) connect with the central retinal vein. Scale bar, 100 µm. ***B***, *In vivo* confocal line-scan images of vessels in the retina, labeled by intravenous injection of FITC dextran. For line-scan images of capillaries (***B1***), vessel diameter is calculated as the distance between the borders of the vessel lumen (red dots). Segments in which diameter cannot be measured accurately (yellow dots) are ignored. Flux is measured by counting the passage of single RBCs (black vertical lines). In larger vessels, diameter is also measured as the distance between the borders of the vessel lumen (***B2***; red dots), and flux is calculated by counting the passage of fluorescently labeled RBCs, imaged at a different wavelength (***B3***; bright vertical lines).

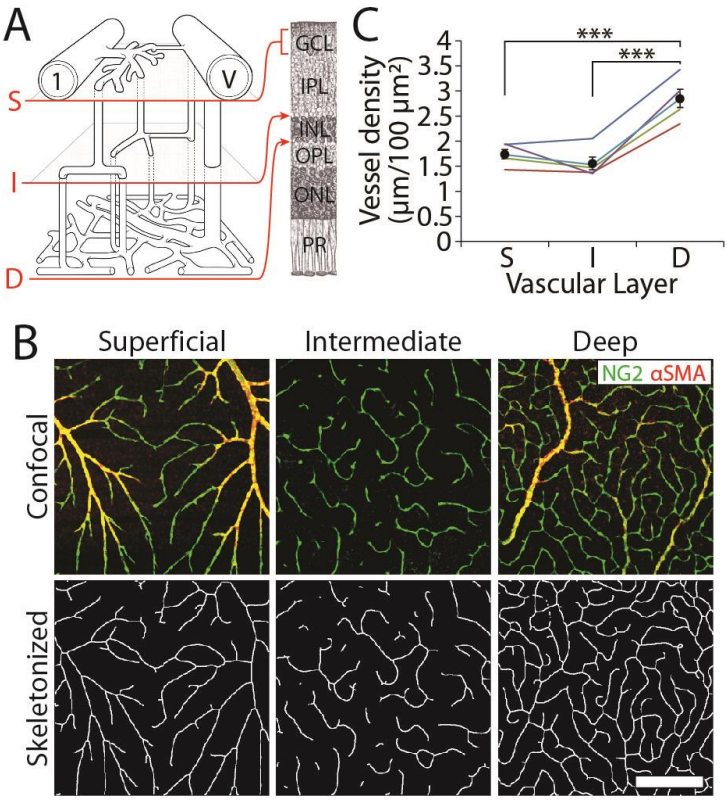

Figure 4.2. Vessel density in the three vascular layers. ***A***, Schematic of the trilaminar vascular network showing the first-order arteriole (1) and venule (V) and the connectivity of the superficial (S), intermediate (I), and deep (D) vascular layers and their locations within the retina. GCL, Ganglion cell layer; IPL, inner plexiform layer; INL, inner nuclear layer; OPL, outer plexiform layer; ONL, outer nuclear layer; PR, photoreceptors. Drawing modified from Paques et al. (2003). ***B***, Top row, Representative confocal images of the superficial, intermediate, and deep vascular layers, labeled for NG2 (green) and α-SMA (red). Bottom row, The images are skeletonized for calculation of vessel density. Scale bar, 200 µm. ***C***, Vessel density in the three vascular layers, measured in five retinas. ***$p < 0.001$.

Vessel density in the trilaminar vascular network

We quantified the density of blood vessels in each of the three vascular layers in the rat retina. Immunohistochemically labeled images of the superficial, intermediate, and deep vascular layers were skeletonized (Fig. 4.2*B*), and the linear density of the vessels in each layer was quantified ($n = 5$ retinas). The vast majority of vessels analyzed were

capillaries, although some second and third-order arterioles were present in the superficial vascular layer, and draining venules were occasionally present in the deep vascular layer. The deep vascular layer had the highest linear density of the three layers (2.85 ± 0.18 μm/100 μm^2; $p < 0.001$), whereas the superficial and intermediate vascular layer densities did not differ (1.74 ± 0.10 and 1.56 ± 0.13 μm/100 μm^2; Fig. 4.2*C*). These values are very similar to those measured in adult mice (Ganesan et al., 2010, 2011) and humans (Tan et al., 2012).

The total blood volume in the three vascular layers can be estimated by multiplying the mean cross-sectional area of the blood vessels in each layer by the linear vascular density in that layer. The mean baseline diameters of arterioles, capillaries, and venules are given in Figure 4.3*C* and Table 4.1. We find that total blood volume in the superficial, intermediate, and deep layers is 41.3, 28.2, and 65.3 μm^3/100 μm^2, respectively. These values are only estimates because they do not include the arterioles of the superficial layer or the draining venules of the deep layer.

Table 4.1: Vessel Properties

	Arterioles			**Capillaries**			**Venules**
Vessel order	**1**	**2**	**3**	**S**	**I**	**D**	**V**
Number of series (number of rats)	17 (*16*)	17 (*13*)	29 (*22*)	74 (*33*)	29 (*18*)	18 (*12*)	12 (*12*)
Baseline diameter (μm)	28.1 ± 1.0	10.5 ± 0.8	7.6 ± 0.4	5.5 ± 0.1	4.8 ± 0.1	5.4 ± 0.2	39.7 ± 3.1
Dilation (%)	7.5 ± 0.7	5.0 ± 0.9	2.7 ± 0.4	1.8 ± 0.2	2.3 ± 0.2	1.9 ± 0.3	1.1 ± 0.2
% responding	100.0	91.7	85.7	75.7	93.1	61.1	100.0

Table 4.1. Vessel properties. Vessel orders 1, 2, and 3 are the first, second, and third branches off the central retinal artery. S, superficial layer vessels of order 4 and higher, defined as capillaries. I, intermediate layer capillaries. D, deep layer capillaries. V, venules are the first branch off the central retinal vein. Dilation, mean dilation during the first 4 s of the stimulus. % responding, percent of series that showed stimulus-evoked dilations that rose at least 3 standard deviations above baseline.

Retinal vessels dilate in response to flicker stimulation

We used a 5 Hz diffuse flickering light to evoke functional hyperemia, a stimulus that is known to effectively activate neurons in the inner retina (Miller, 2001). The

magnitude of flicker-evoked dilation differed according to vessel order. In the superficial vascular layer, response amplitude decreased with vessel order, with the largest dilations seen in first-order arterioles (Fig. 4.3 *A*, *B*, *D*). The response profile of vessel dilation also varied according to vessel order. First-, second-, and third-order arterioles displayed a clear biphasic response (Fig. 4.3*A*), with a first peak occurring within a few seconds of light onset and a second phase developing slowly and peaking at ~13 s after light onset. Superficial capillaries and venules had more subtle biphasic response profiles. We have observed previously similar flicker-evoked biphasic increases in diameter (Mishra and Newman, 2011), Muller cell Ca^{2+} signaling (Newman, 2005), and blood velocity (Srienc et al., 2010) in the rat. In contrast, biphasic responses have not been observed in the cat (Buerk et al., 1995) and human (Garhöfer et al., 2003; Polak et al., 2002) retinas. When we quantified dilation as the percentage increase in diameter during the first 4 s after light onset (capturing the first peak), we found that dilations in the first-order arterioles were larger than in third-order arterioles and all other downstream vessels ($p < 0.001$; Fig. 4.3*D*, Table 4.1). The second-order arteriole dilations were larger than superficial capillaries and venules ($p < 0.01$).

We then compared the dilatory responses of capillaries in the three vascular layers. Unexpectedly, we found dramatic differences in flicker-evoked capillary dilation in the three layers (Fig. 4.3*E*–*G*). The time courses of flicker-evoked capillary dilation were strikingly different. Dilation of superficial layer capillaries resembled the biphasic dilatory response of upstream arterioles, whereas dilation of deep layer capillaries resembled the downstream venule response. In contrast, the slow, continuously increasing dilation of intermediate layer capillaries resembled neither the responses of superficial or deep layer capillaries nor the responses of arterioles or venules. To quantify the capillary responses in the three vascular layers, we calculated the mean dilation during the entire 15 s stimulus. Intermediate layer capillaries dilated more than twice as much as superficial and deep layer capillaries (2.55 ± 0.30 vs 0.89 ± 0.16 and 0.66 ± 0.28%; $p < 0.001$; Fig. 4.3*G*). In summary, we find that arterioles dilate more than other retinal vessels and likely drive blood flow in the retinal vasculature. Furthermore, the large, slow dilations of capillaries in the intermediate vascular layer suggest the presence

of a unique regulatory mechanism.

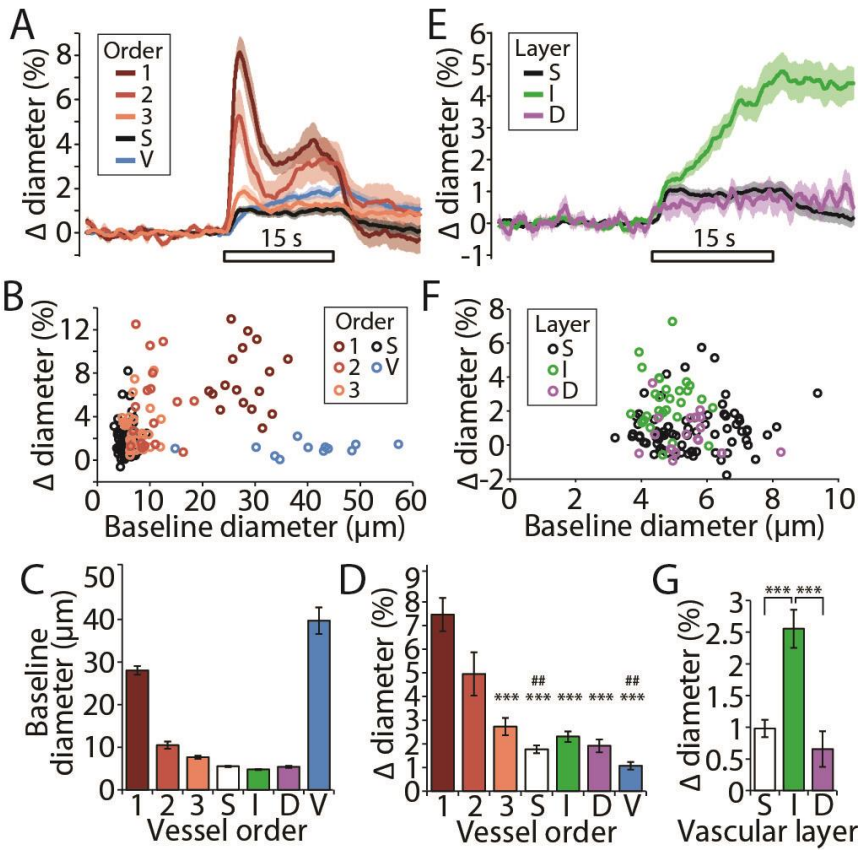

Figure 4.3. Flicker-evoked dilation of retinal vessels. ***A***, Time course of flicker-evoked dilation of superficial layer vessels. Mean ± SEM are shown. The open horizontal bar in this and other figures indicates the flicker stimulus. ***B***, Scatter plot of flicker-evoked vasodilation (maximum change during the first 4 s of stimulation) versus baseline vessel diameter for superficial layer vessels. Data are color coded by vessel order. ***C***, Mean baseline diameter of retinal vessels by vessel order. ***D***, Mean flicker-evoked dilation (maximum change during the first 4 s of stimulation) by vessel order. ***$p < 0.001$, compared with first order; ##$p < 0.01$, compared with second order. ***E***, Time course of flicker-evoked dilation in the three vascular layers. ***F***, Scatter plot of flicker-evoked vasodilation (mean dilation during the 15 s stimulus) versus baseline vessel diameter for the three vascular layers. ***G***, Mean flicker-evoked dilations for the three vascular layers. ***$p < 0.001$. Order 1-3 vessels are in the superficial vascular layer. D, deep layer capillaries; I, intermediate layer capillaries; S, superficial layer capillaries (order 4 and higher vessels); V, venule. Abbreviations apply to subsequent figures.

Arterioles respond rapidly and consistently to flicker stimulation

The location within the vascular network in which functional hyperemia is initiated remains an open question. In the brain, evidence suggests that blood flow first increases in the middle cortical layers before spreading toward the pial surface (Lindvere et al., 2013; Silva and Koretsky, 2002; Tian et al., 2010), although it remains to be determined which vessels are responsible for the initial increase (Hall et al., 2014). We found that, in the retina, arterioles dilate more reliably and faster than downstream capillaries and venules. We first calculated the fraction of vessels that dilated in response to a flicker stimulus. Vessels were considered to respond if their diameter during the stimulus rose at least 3 SDs above baseline. First-order arterioles responded 100% of the time (n = 7). The likelihood of vessel dilation tended to decrease with distance along the vascular tree (Fig. 4.4*A*, Table 4.1). The percentage of vessels responding was 92% (n = 12) for second-order arterioles and fell to as low as 61% (n = 18) for capillaries in the deep vascular layer. Deviating from this trend, 93% (n = 29) of capillaries in the intermediate layer and 100% (n = 5) of venules dilated.

We calculated the time at which vessels began to dilate, the onset time, to determine which vessels responded first to flicker stimulation. We first estimated the onset time by examining the average response profile for each type of vessel (Fig. 4.4*B*). When these traces were normalized to the peak response (Fig. 4.4*C*), we observed that first and second-order arterioles dilate most rapidly. Venules had a noticeable delay in their rising phase. A more quantitative assessment was obtained by defining onset as the time it takes for a vessel to reach 20% of its peak dilation (Fig. 4.4*D*). There was a general trend for onset time to be shortest for first-, second-, and third-order arterioles (0.73 ± 0.08, 0.70 ± 0.16, and 0.60 ± 0.34 s, n = 7, 11, and 23, respectively) and longer for superficial capillaries (0.97 ± 0.49 s, n = 46). Venules had the longest onset time (1.06 ± 0.49 s, n = 5). However, none of these groups were significantly different from each other.

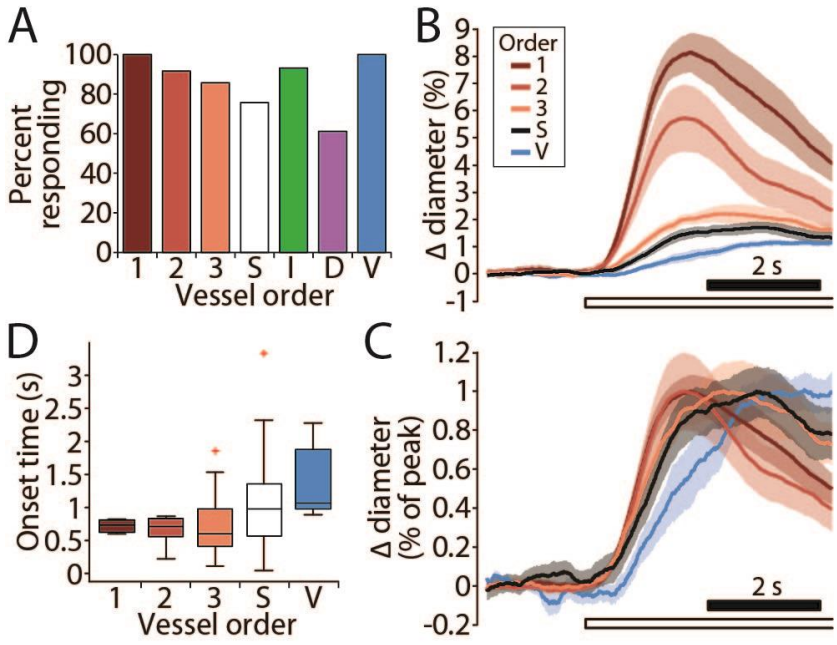

Figure 4.4. Flicker-evoked response frequency and onset time in the retinal vasculature. ***A***, Percentage of vessels responding to flicker stimulation, defined as a response >3 SDs above baseline. ***B***, Time course of flicker-evoked dilation of vessels in the superficial vascular layer. Note that the flicker stimulus (open bar) continues beyond the end of the traces. ***C***, Vessel diameter traces in ***B*** are normalized for comparison of onset times. ***D***, The onset time of vessels of different order, shown as box plots, with the * symbol indicating outliers. For details of onset time calculation, see Materials and Methods.

RBC flux increases in response to flicker stimulation

RBC flux is a direct and sensitive measure of blood flow. If functional hyperemia is controlled solely by the active dilation of retinal arterioles, then the flicker-evoked RBC flux increase in all downstream vessels should be equal. However, this was not what we observed. RBC flux in first-order arterioles and venules, measured using ultrafast line scans with a 2 s flicker stimulus, increased to a peak value of 11% and had nearly identical time courses (Fig. 4.5*A*). RBC flux in smaller vessels was measured with standard line scans and a 15 s flicker stimulus. Although the initial flicker-evoked flux increase was equal in second and third-order arterioles and superficial capillaries, flux changes during the second phase of the response decreased with vessel order (Fig. 4.5*B*).

We calculated the mean flicker-evoked RBC flux change in superficial layer vessels during the first 2 s of the stimulus. Restricting our analysis to the first 2 s allowed us to include short trials in which only a 2 s stimulus was used. Light-evoked flux increases averaged 4.67 ± 1.71% (n = 8) in first-order arterioles, 8.19 ± 0.71% (n = 5) in second-order arterioles, 6.74 ± 0.75% (n = 6) in third-order arterioles, 11.33 ± 1.47% (n = 32) in capillaries, and 3.94 ± 1.71 (n = 8) in venules (Fig. 4.5*C*, *D*). These flux increases were not significantly different from each other.

We then characterized flux in the capillaries of the three vascular layers. Baseline flux in superficial, intermediate, and deep vascular layers did not differ (61.0 ± 5.3, 42.2 ± 3.2, and 39.4 ± 3.2 RBCs/s, n = 32, 18, and 12, respectively; Fig. 4.5*G*). However, flicker-evoked flux increases were dramatically different (Fig. 4.5 *E*, *F*, *H*). When averaged over the 15 s stimulus period, the flux increase in the intermediate vascular layer was much greater than the increases in the superficial and deep layers (25.65 ± 5.16 vs 0.82 ± 2.17 and 11.27 ± 2.85%; $p < 0.001$ and $p < 0.05$, respectively; Fig. 4.5*H*).

The time course of flicker-evoked capillary flux changes also differed in the three vascular layers (Fig. 4.5*E*). After an initial peak, flux in intermediate capillaries continued to rise throughout the stimulus period, similar to the intermediate layer dilatory response (Fig. 4.3*E*). The time course of the flux increase in the deep capillaries also paralleled the dilation in vessels of the deep vascular layer. However, the flux change in superficial layer capillaries did not match the dilatory response. This was particularly evident at the end of the 15 s stimulus period. At this time, flux had increased by 34% in the intermediate vascular layer and 10% in the deep capillary layer. Strikingly, flux had actually decreased by 7% in the superficial capillaries. Because the superficial capillaries remained dilated for the duration of the stimulus, the decrease in flux must reflect a decrease in perfusion pressure in these vessels. This is likely attributable to the diversion of flow to the intermediate and deep layer capillaries.

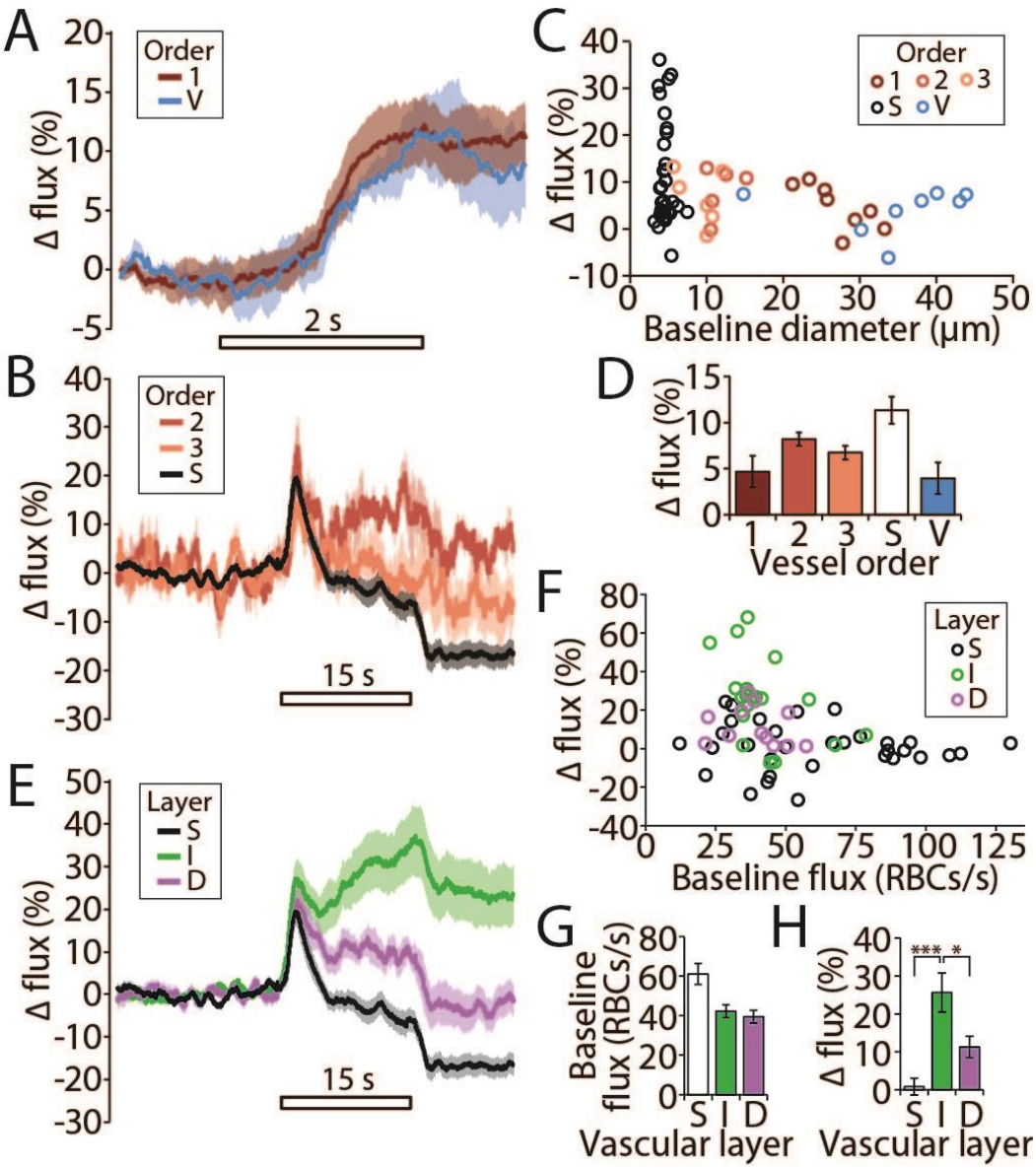

Figure 4.5. Flicker-evoked increases in RBC flux. ***A***, Time course of flicker-evoked RBC flux increases in first-order arterioles and venules. ***B***, Time course of RBC flux increase in secondand third-order vessels and superficial layer capillaries (S). ***C***, Scatter plot of RBC flux increase (mean during the first 2 s of stimulation) versus baseline vessel diameter, color coded by vessel order. ***D***, Mean increase in flicker-evoked RBC flux (mean during the first 2 s of stimulation) by vessel order. ***E***, Time course of RBC flux increases in the capillaries of the three vascular layers. ***F***, Scatter plot of RBC flux increases in capillaries (mean during the 15 s stimulus) versus baseline flux in the three vascular layers. ***G***, ***H***, Baseline RBC flux (***G***) and flux increases (***H***) for capillaries in the three vascular layers. *$p < 0.05$; ***$p < 0.001$.

Pericyte proximity does not predict dilation amplitude

Active regulation of blood flow in capillaries remains a controversial issue (Fernández-Klett et al., 2010; Hall et al., 2014). Active regulation in capillaries would occur via pericytes, because they are the only contractile cells associated with these vessels. We tested whether pericytes in the retina actively regulate blood flow by measuring flicker-evoked capillary dilation as a function of distance from pericyte somata. If pericytes actively regulate blood flow, we would expect flicker evoked dilation to be greater near pericyte somata, where the circumferential pericyte processes are located, rather than farther away (Dore-Duffy and Cleary, 2011; Kotecki et al., 2010; Nehls and Drenckhahn, 1991; Peppiatt et al., 2006).

We measured flicker-evoked capillary dilation at different sites along capillaries in the three vascular layers. After *in vivo* experimentation, retinas were removed and labeled for the chondroitin sulfate proteoglycan NG2 to localize pericyte somata, which appeared as protrusions from the capillary wall (Fig. 4.6*A*, arrowheads). *In vivo* and whole-mount images of the same retinal regions were aligned, and the distance from each *in vivo* measurement site to the nearest pericyte soma was determined. Linear regression analysis showed that the distance from a pericyte was not predictive of the magnitude of capillary dilation, when either all capillaries were pooled together ($p < 0.20$, $n = 105$) or capillaries in each vascular layer were tested separately ($p < 0.26$ in the superficial layer, $n = 62$; $p < 0.91$ in the intermediate layer, $n = 27$; $p < 0.12$ in the deep layer, $n = 16$; Fig. 4.6*B*). Capillary measurements were sorted into one of three groups according to their distance from a pericyte soma: close (<10 μm), medium (≥10 and <25 μm), or far (≥25 μm). No clear difference in response amplitude was observed between these groups in any of the vascular layers ($n = 17$, 31, and 14 for the superficial layer, $n = 5$, 11, and 11 for the intermediate layer, and $n = 5$, 7, and 4 for the deep layer; Fig. 4.6*C*).

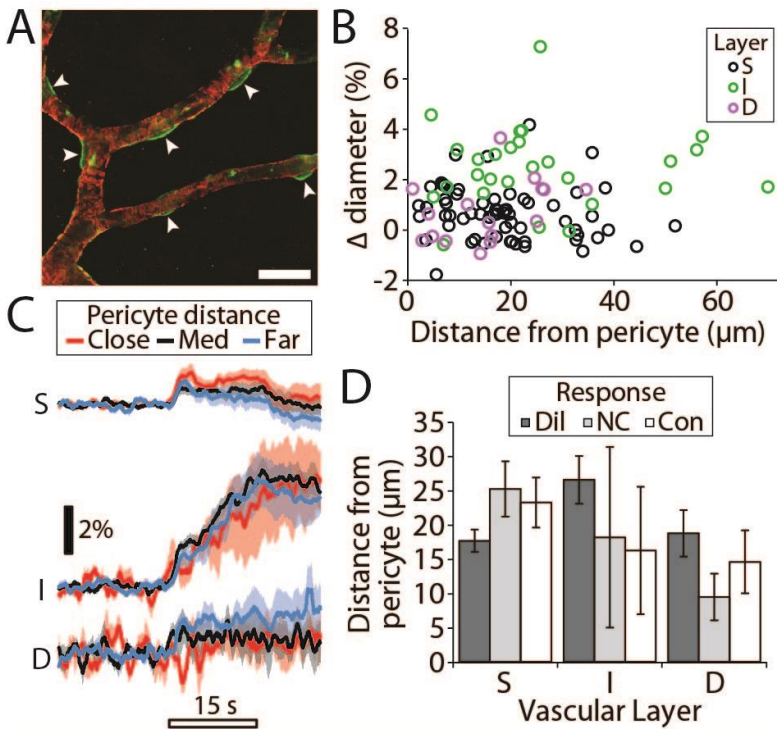

Figure 4.6. Pericyte proximity does not determine dilation amplitude. ***A***, Whole-mount confocal image of superficial layer vessels labeled for α-SMA (red) and NG2 (green). Pericyte somata are indicated by arrowheads. Scale bar, 20 μm. ***B***, Scatter plot of flicker-evoked dilation versus distance from pericyte somata for capillaries in the three vascular layers. ***C***, Time course of flicker-evoked capillary dilation for each of the three vascular layers, measured at sites close (≤10 μm), at a medium distance (>10 and ≤ 25 μm), and far (>25 μm) from pericyte somata. *D*, Mean distance from pericyte somata for capillaries in each vascular layer that responded to flicker with a dilation (Dil), a constriction (Con), or no change in diameter (NC).

Another way of comparing vascular responses to the proximity of pericytes is to classify each response as dilating, constricting, or not changing. Responses were classified as dilating or constricting if the peak positive or negative response was at least 3 SDs above or below the baseline. There was no difference in the mean distance to pericytes for the three response groups, when either all capillaries were pooled together or each layer was considered separately (Fig. 4.6*D*). These results are discussed below in the context of our other findings.

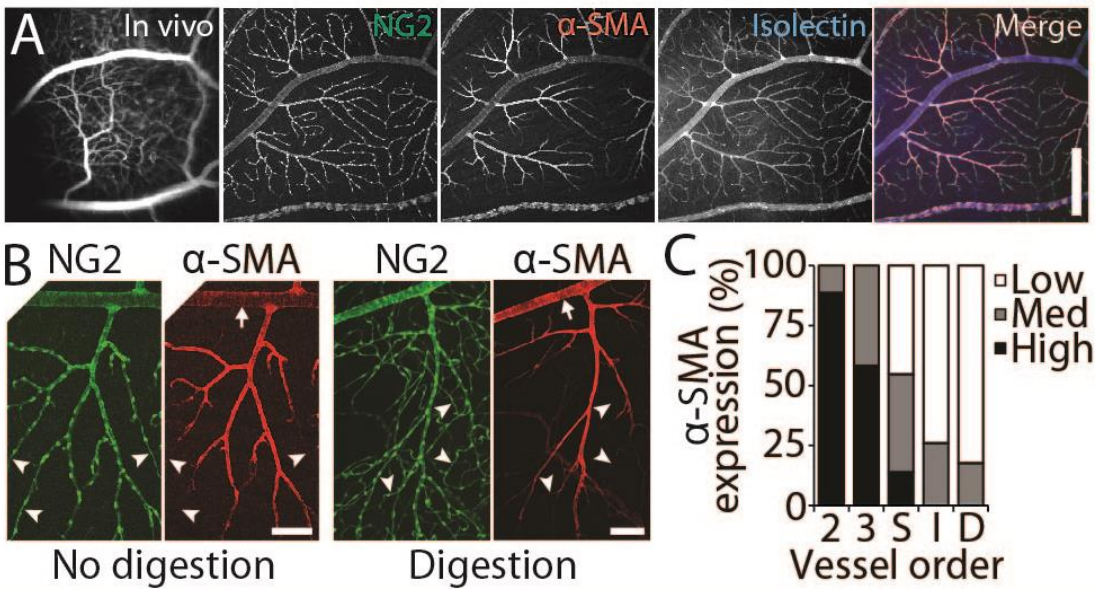

Figure 4.7. Expression of α-SMA decreases with increasing vessel order in the retinal vasculature. ***A***, A retinal region imaged *in vivo* (first panel) and as a whole-mount, labeled for the pericyte marker NG2, the contractile protein α-SMA, and with the vessel marker Isolectin-IB4. The three labels are merged in the last panel. Scale bar, 400 μm. ***B***, Retinal vessels are labeled for NG2 and α-SMA with no enzymatic digestion (left panels) and with digestion with collagenase/dispase (right panels). Arrows indicate first-order vessels in which strong α-SMA labeling is observed after enzyme digestion. High branch order vessels often express low levels of α-SMA (arrowheads). Scale bars, 100 μm. ***C***, The strength of α-SMA expression (low, medium, or high) is indicated for vessels of each order.

α-SMA expression reflects vascular responsiveness

α-SMA is a contractile protein expressed in pericytes and in the vascular smooth muscle cells that surround arteries and arterioles. Its level of expression has been correlated with the degree of vascular contractility in rat and mouse (Hinz et al., 2001; Schildmeyer et al., 2000; Tomasek et al., 2006). Other reports indicate that a subset of capillary pericytes express α-SMA (Bandopadhyay et al., 2001; Nehls and Drenckhahn, 1991), but we could not resolve α-SMA labeling to the level of individual pericytes. Instead, we categorized each vessel segment that was investigated *in vivo* as expressing high, medium, or low levels of α-SMA. In agreement with previously published work (Hughes and Chan-Ling, 2004; Nehls and Drenckhahn, 1991), we found that α-SMA expression decreased with increasing vessel order (Fig. 4.7) and was often undetectable

in the smallest capillaries (Fig. 4.7*B*, arrowheads). α-SMA expression levels were lower in the intermediate and deep vascular layers than in the superficial vessels (Fig. 4.7*C*), although this may have been attributable to reduced antibody penetrance. In our initial studies using a standard immunohistochemistry protocol, α-SMA expression was unexpectedly low in most regions of first-order arterioles compared with second-order arterioles. Collagenase/dispase digestion of the retina before performing immunohistochemistry increased antibody penetration, and we observed more regions of high α-SMA labeling in the first-order arterioles (Fig. 4.7*B*, arrows). Enzyme digestion did not disrupt the binding of other antibodies, nor did it change the observation that α-SMA expression decreases with vessel order.

Discussion

Active dilation of arterioles drives functional hyperemia in the retina

We have found that flickering light evokes large, rapid, and consistent dilations in retinal arterioles but smaller, slower, and inconsistent dilations in downstream capillaries and venules. Retinal arterioles are also highly enriched with α-SMA, a protein whose expression levels correlate with contractility (Hinz et al., 2001; Schildmeyer et al., 2000; Tomasek et al., 2006). Together, these results indicate that functional hyperemia in the retina is driven principally by the active dilation of arterioles. Although the initial transient dilation in downstream capillaries and venules is likely attributable to passive stretch, we propose that more complex regulatory mechanisms are at play during prolonged stimulation. These mechanisms, discussed below, can account for the differential blood flow responses we observed in the three vascular layers.

Flicker stimulation evoked small dilations in venules compared with arterioles in our experiments. In the human retina, in contrast, venule and arteriole dilations are of similar magnitude (Garhöfer et al., 2004b; Hammer et al., 2011; Noonan et al., 2013; Polak et al., 2002). The difference could arise because venule diameters are only ~21% larger than arteriole diameters in humans but 41% larger in our rats. Thus, human venules

may need to dilate more than rat venules to accommodate the same increase in blood flow.

Baseline blood flow in the three vascular layers

The intermediate vascular layer vessels had the smallest total blood vessel volume and approximately the same baseline flux as the other two vascular layers, indicating that total baseline blood flow was lower in the intermediate layer than in the other two vascular layers. This is consistent with intraretinal pO_2 measurements, which reveal high pO_2 near the surface of the rat retina and in the region near the deep vascular layer and lower pO_2 in the region near the intermediate vascular layer (Lau and Linsenmeier, 2012). Although intermediate layer blood flow is low at baseline, it is likely adequate to support the metabolic needs of the inner retina during constant dim illumination (Miller, 2001).

Differential regulation of blood flow in the three vascular layers

We observed a striking difference in flicker-evoked regulation of capillary blood flow in the three vascular layers of the retina. Stimulation evoked much larger dilations in intermediate layer capillaries than in capillaries of the superficial and deep vascular layers. At the end of the 15 s stimulus, intermediate layer capillaries had dilated 4.4%. According to a modified version of the Hagen-Poiseuille law (Blinder et al., 2013), which accounts for vessel diameter, as well as the effects of hematocrit and RBC interactions with the vessel wall, a 4.4% dilation translates to a 16.5% decrease in vascular resistance. In comparison, the resistance decrease in the superficial and deep layer capillaries was 3.9 and 3.3%.

The intermediate layer capillary dilation had a unique time course, increasing continually for the duration of the stimulus. Dilation of the superficial and deep layer capillaries, in contrast, remained relatively constant throughout the stimulus. Flicker evoked RBC flux in the intermediate vascular layer continued to rise for the duration of the stimulus, mirroring the dilation observed in intermediate layer capillaries. Averaged over the duration of the stimulus, the intermediate layer flux increase was more than

twice that in the deep capillary layer. In contrast, after a transient increase, flux in the superficial layer capillaries declined steadily during stimulation. Third-order arterioles in the superficial vascular layer showed a similar slow flux decline. The flux decrease in the superficial layer vessels is likely attributable to a "steal" effect (Raichle, 1998), with blood being diverted to the intermediate and deep layer capillaries.

The differential regulation of blood flow in the three vascular layers will affect oxygen and nutrient delivery and may reflect differences in neuronal metabolic demand. The intermediate vascular layer supplies neuronal somata and synapses of the inner retina, which are activated more by changes in luminance than by steady illumination (Miller, 2001). Stimulus-evoked activity results in large increases in neuronal metabolism in this layer (Bill and Sperber, 1990; Lau and Linsenmeier, 2012). The large flicker evoked blood flow increase in intermediate layer capillaries may be necessary to meet the increased metabolism of these neurons. In contrast, the deep vascular layer supplies oxygen and nutrients to the synapses in the outer plexiform layer, which are active under all stimulus conditions. Therefore, there is little metabolic need for large increases in blood flow to the deep vascular layer. The superficial capillary layer primarily supplies the retinal ganglion cells, which are activated by changes in light (Miller, 2001). However, oxygen is supplied to this layer by both the superficial layer vessels and by the vitreous humor, in which pO_2 is higher than in the inner retina (Lau and Linsenmeier, 2012). pO_2 near the retinal surface may be high enough at rest so that there is no need to increase blood flow during stimulation.

Our observations on blood flow in the trilaminar retinal network correspond well with investigations in the cortex. Although the cortex is a stratified tissue, there are no discrete cortical vascular layers as there are in the retina. Nevertheless, fMRI (Goense et al., 2012; Kim and Kim, 2010; Smirnakis et al., 2007), two-photon imaging (Lindvere et al., 2013), laser Doppler flowmetry (Norup Nielsen and Lauritzen, 2001), and autoradiography (Gerrits et al., 2000) studies indicate that sensory stimulation results in greater increases in blood flow in the middle cortical layers, including layer IV, where neuronal and vascular density (Smirnakis et al., 2007) and stimulation induced neuronal signaling are highest. Similar to the retina, this differential regulation of blood flow in the

cortex may serve to supply blood to regions of high metabolic need (Carroll and Wong-Riley, 1984; Goense et al., 2012; Norup Nielsen and Lauritzen, 2001).

Active capillary regulation

The large, slowly developing dilation of intermediate layer capillaries, which differs markedly from the responses of upstream arterioles, is most likely caused by active dilation. Active capillary dilation would account for the unique time course we observed in the intermediate layer capillaries, as well as for the reduction in RBC flux in superficial layer vessels. Although still controversial, studies in several brain regions, including the cortex (Chen et al., 2011), olfactory bulb (Chaigneau et al., 2003), and subventricular zone (Lacar et al., 2012), also suggest that capillaries actively regulate blood flow. Recent observations in the somatosensory cortex provide strong evidence that pericyte relaxation mediates the active capillary response (Hall et al., 2014).

Dilation of intermediate layer capillaries is presumably mediated by active relaxation of the pericytes on these vessels. However, we found no evidence for active pericyte dilation of capillaries. Furthermore, we found that α-SMA expression in the intermediate and deep layer capillaries is lower than in superficial layer vessels. These apparently contradictory findings could be attributable to several factors. First, our assumption that pericyte-mediated dilation is greater near pericyte somata than farther away could be false. This possibility is supported by recent observations in the cortex (Hall et al., 2014), where capillary dilations at pericyte somata and processes were equal but were smaller where pericytes were absent. In the retina, where pericyte density is higher than in the cortex (Frank et al., 1987), it is difficult to find regions where pericytes are absent. Given that we used a diffuse stimulus to activate the retina, that retinal pericytes are closely spaced, and that they are electrically coupled (Puro, 2007), it is not surprising that all regions of capillaries with pericyte coverage dilate to a similar extent. Second, we did not characterize flicker-evoked dilation in the diving capillaries connecting superficial layer vessels to intermediate and deep layer capillaries. It is possible that pericyte-mediated dilations are present in these vessels. Third, although α-SMA expression in the intermediate and deep layer capillaries is low, capillary pericytes

may express enough actin to mediate active responses. The low levels of α-SMA expression we observed in capillaries may account for their slow dilations. Pericytes may also express other actin isoforms (Tomasek et al., 2006), although their role in capillary dilation is unclear.

Passive capillary regulation

We propose that the slow dilation observed in the intermediate layer capillaries is attributable to active dilation of the vessels. However, passive stretch may also contribute to this response. The time course of the dilation is similar to blood volume increases measured in the brain in response to sensory stimulation (Barrett et al., 2012; Drew et al., 2011; Mandeville et al., 1999). These slow volume increases have been attributed to the windkessel effect, in which active arteriole dilation results in a pressure increase that passively dilates downstream vessels (Barrett et al., 2012; Drew et al., 2011; Huppert et al., 2007; Kong et al., 2004; Mandeville et al., 1999). The windkessel effect does not, in itself, account for differential dilation of the three capillary layers. Several other factors could contribute to differential dilation. First, intermediate layer capillaries, which have a smaller total volume than capillaries in the other two layers, would also have a higher resistance. Dilation of upstream arterioles would generate greater pressure increases in intermediate layer capillaries, leading to larger passive stretch. Second, capillaries in the intermediate layer could have a higher compliance, resulting in greater stretch for a given pressure increase.

Conclusions

Our results indicate that arterioles are primarily responsible for generating functional hyperemia in the retina. These vessels display large, rapid, and consistent flicker-evoked dilations and high α-SMA expression. We also found that blood flow through the three vascular layers in the retina is differentially regulated. Prolonged flicker stimulation evokes a large, slowly developing dilation and an increase in flux in intermediate layer capillaries that are not observed in the other two vascular layers. Active capillary dilation likely contributes to this response.

Chapter 5: General discussion

Relevance of current work to functional imaging techniques

Investigating blood flow in human brains requires non-invasive and easily tolerated tools. Many instruments have been developed for assessing blood flow in the retina (Chapter 3) but few exist to study blood flow in the brain. The most common of these is functional magnetic resonance imaging (fMRI), which typically uses blood-oxygen-level dependent contrast (BOLD) signals to detect the changes in blood oxygenation that occur following neuronal activity. The problem with this technique is that the relationship between neuronal signaling and blood oxygenation is anything but straightforward. The research presented here provides insight into the underlying mechanisms of functional hyperemia, and can inform the ongoing discussion about how to interpret BOLD signals.

A positive BOLD signal is due to the counterintuitive decrease in oxygen extraction fraction, and accompanying decrease in deoxyhemoglobin, that occurs when blood flow increases during functional hyperemia. A complete discussion of the underpinnings of BOLD is out of the scope of this dissertation. However, there are many caveats to interpreting BOLD signals as neuronal activity (reviewed by Buxton (2010) and Buxton et al (2014)). Some caveats applicable to the current work have already been mentioned. First, neurovascular coupling mechanisms are themselves complex and redundant: both neurons and glial cells communicate with the vasculature via multiple pathways simultaneously, the combination of which may differ depending on circumstance. Second, functional hyperemia is a feed forward mechanism, so there should be no expectation that changes in blood flow will perfectly mirror neuronal need. Third, comparing BOLD signals across different brain regions is problematic since different vascular density will affect BOLD signals, and sparsely vascularized areas might not generate blood flow signals that are detectable with current methods.

A major open question is how the microvasculature plays into functional hyperemia response as it is detected by neuroimaging. Not only does functional hyperemia rely on healthy neuronal signaling pathways, it likely also requires healthy

glial cells and pericytes. Further, the BOLD response can vary widely both across the cortical surface (Ances et al., 2008) and within its depth. Blood flow has been shown to increase first in the deeper layers and propagate toward the surface (Chen et al., 2011; Lindvere et al., 2013; Tian et al., 2010). But by averaging the BOLD signal across the depth of the cortex or only looking at the brain's surface, where large draining veins are present, we may miss important information about the spatial and temporal dynamics of brain signaling. As the resolution of fMRI instruments increases, it may become possible to visualize very spatially discrete changes in blood flow due to capillary dilation. To better interpret neuroimaging data, it is important to consider complete vascular units, which include arteries, veins, and the microvasculature between them, which span the full cortical depth (Harel et al., 2010; Huber et al., 2014; Kennerley et al., 2010).

We made the novel observation that the retinal vascular layers are differentially regulated and found that dilation onset time scaled approximately with vessel order. Another group's similar study showed that pericyte-mediated capillary dilations preceded dilations of upstream vessels (Hall et al., 2014). This indicates that the mechanisms behind functional hyperemia may not be identical in the retina and the cortex, a conclusion that should be unsurprising given the differences between these two tissues. Regardless, the observation that microvascular blood flow can be autonomously mediated implies that a significant portion of the BOLD signal is due to active capillary dilations. Reductions in the BOLD response in disease populations may well be a reflection of the health of non-neuronal cell types including glia and pericytes, or the state of the microvasculature.

Directions of future research

We have shown that the three retinal vascular layers have distinct functional hyperemia response profiles. However, we are left to speculate about the underlying cause of the differential blood flow response. As discussed in Chapter 4, passive mechanisms may account for some of the differential blood flow response. Differences in baseline vessel diameter, resistance, compliance, or density in each of the three vascular layers would affect their passive reaction to changes in upstream blood pressure.

However, we suspect that pericytes, at least in part, drive the large dilations of intermediate layer capillaries. Further work will be needed to definitively determine whether this response is passive, active, or some combination thereof. Additionally, we are interested in knowing the molecular mechanisms underlying this response.

A thorough modeling study could shed light on the source of the slowly developing blood flow increase in the intermediate layer. By accurately representing the connectivity of the three vascular layers and manipulating basic morphological properties of the blood vessels in the three layers, it would be possible to assess the likelihood that this response requires active capillary dilation. The retinal vascular network has been modeled previously (Arciero et al., 2013; Ganesan et al., 2010, 2011). However, blood flow within the network has only been investigated under baseline conditions (Guidoboni et al., 2014), not during functional activation. A more complete modeling study could reveal the combination of parameters necessary to generate the functional hyperemia responses we observed.

If modeling studies show that capillaries must actively dilate in order to generate the observed blood flow response, many questions remain. Because pericytes are the only cells present on capillaries with known contractile abilities, it is expected that they provide the muscular force required to dilate capillaries. However, this would raise additional questions. First, what cell type is responsible for signaling metabolic need to pericytes? Neurons or glial cells, or some combination of the two, could relay the metabolic state of nearby neurons to pericytes. Second, if pericytes are present on capillaries in all three vascular layers, and it appears they are, why does the intermediate layer dilate to a much greater extent than the other two layers? It could be that intermediate layer pericytes are somehow different than those in other layers; perhaps they have more functional contractile machinery, or they express a complement of receptors that make them particularly sensitive to nearby neuronal signaling. Or, pericytes may be the same in all retinal capillaries, but they are exposed to different levels of activity depending on their laminar position. Neurons in the outer sublamina of the inner plexiform layer have a high metabolic need compared with other regions of the middle retina (Yu and Cringle, 2001), and vasodilatory signals from the inner plexiform

layer may be spatially limited such that they affect only the intermediate vascular layer. Whether pericyte heterogeneity and/or differences in neuronal need drive the retina's differential functional hyperemia response remains to be parsed out.

Measuring tissue oxygen consumption allows us to approximate the blood flow required to meet local oxygen demand. The oxygen profile of the retina has been investigated using oxygen probes during dark and light adaptation, and the oxygen consumption rates of each retinal layer have been modeled (Yu and Cringle, 2001). However, the laminar changes in oxygen content that occur during a flickering light stimuli like the one applied here (Chapter 4) have not been fully investigated. Oxygen in the inner retina drops more in response to a flickering than a steady light stimulus (Lau and Linsenmeier 2012), but the authors of this study did not report the oxygen levels for separate inner retinal layers. Based on our data, we would expect that the OFF sublamina of the inner plexiform layer, adjacent to the intermediate vascular layer, would have a larger increase in activity than the outer section of the outer plexiform layer or the outer plexiform layer. Further, we expect that this oxygen need would be maintained with continued flicker stimulation, driving a consistent rise in intermediate layer blood flow. It will be interesting to see if these expectations are met.

The work presented in this dissertation provides the first indication that blood flow is differentially regulated in the three layers of the retinal vasculature. As such, a great deal of work remains to be done to parse out the mechanisms that give rise to this observation.

Summary of presented work

The work discussed in this dissertation provides novel insights into the regulation of blood flow in the retinal vascular network. These studies were made possible by techniques we developed that are capable of measuring relative and absolute blood flow. These techniques are based on direct observations of fRBCs moving through vessels. We used ultra-fast confocal line scans to reach the temporal resolution required to capture high-velocity cells flowing through large vessels. We demonstrated that this technique provides accurate and reliable blood flow measurements. This allowed us to observe

numerous principles of blood flow directly. Among them is the ability to quantify total retinal blood flow in the rat, corroborating estimates from other groups, and to observe parabolic velocity profiles across retinal blood vessels between 20 to 30 μm in diameter.

We measured baseline and flicker-evoked blood flow in vessels throughout the retinal vascular network and concluded that retinal blood flow increases are driven primarily by the large, fast, and consistent dilations of retinal arterioles. Intriguingly, the blood flow response in the intermediate vascular layer was much greater than in the other vascular layers and displayed a unique, slowly developing response profile that was unlike the blood flow response in any other retinal vessel type. This indicates that capillary diameters are actively regulated in response to neuronal need. This differential response has important implications for our understanding of blood flow regulation.

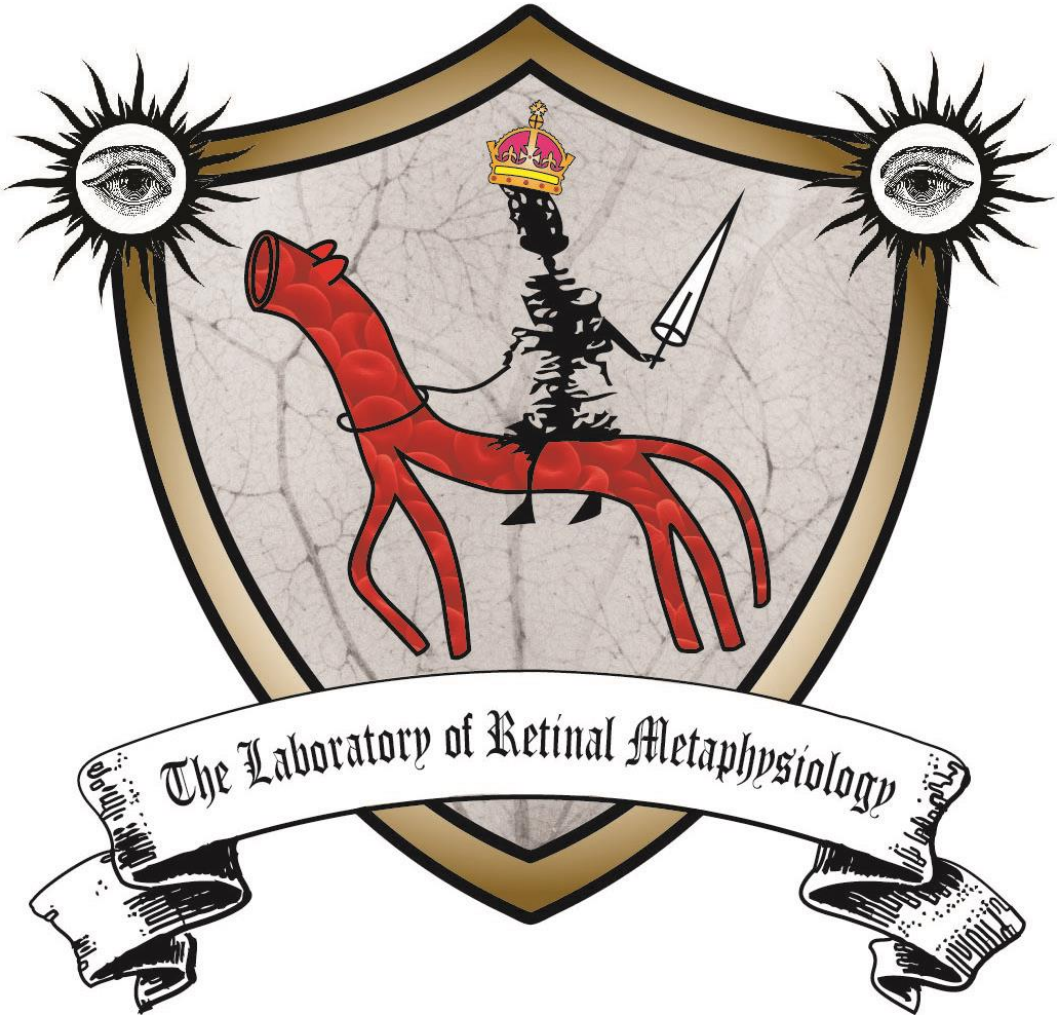
The Laboratory of Retinal Metaphysiology

References

Ahmed, J., Pulfer, M.K., and Linsenmeier, R.A. (2001). Measurement of blood flow through the retinal circulation of the cat during normoxia and hypoxemia using fluorescent microspheres. Microvasc. Res. *62*, 143–153.

Alder, V.A., Cringle, S.J., and Constable, I.J. (1983). The retinal oxygen profile in cats. Invest. Ophthalmol. Vis. Sci. *24*, 30–36.

Alliot, F., Rutin, J., Leenen, P.J., and Pessac, B. (1999). Pericytes and periendothelial cells of brain parenchyma vessels co-express aminopeptidase N, aminopeptidase A, and nestin. J. Neurosci. Res. *58*, 367–378.

Ances, B.M., Leontiev, O., Perthen, J.E., Liang, C., Lansing, A.E., and Buxton, R.B. (2008). Regional differences in the coupling of cerebral blood flow and oxygen metabolism changes in response to activation: implications for BOLD-fMRI. NeuroImage *39*, 1510–1521.

Arciero, J., Harris, A., Siesky, B., Amireskandari, A., Gershuny, V., Pickrell, A., and Guidoboni, G. (2013). Theoretical analysis of vascular regulatory mechanisms contributing to retinal blood flow autoregulation. Invest. Ophthalmol. Vis. Sci. *54*, 5584–5593.

Armulik, A., Genové, G., Mäe, M., Nisancioglu, M.H., Wallgard, E., Niaudet, C., He, L., Norlin, J., Lindblom, P., Strittmatter, K., et al. (2010). Pericytes regulate the blood-brain barrier. Nature *468*, 557–561.

Armulik, A., Genové, G., and Betsholtz, C. (2011). Pericytes: developmental, physiological, and pathological perspectives, problems, and promises. Dev. Cell *21*, 193–215.

Attwell, D., Buchan, A.M., Charpak, S., Lauritzen, M., Macvicar, B.A., and Newman, E.A. (2010). Glial and neuronal control of brain blood flow. Nature *468*, 232–243.

Autio, J., Kawaguchi, H., Saito, S., Aoki, I., Obata, T., Masamoto, K., and Kanno, I. (2011). Spatial frequency-based analysis of mean red blood cell speed in single microvessels: investigation of microvascular perfusion in rat cerebral cortex. PloS One *6*, e24056.

Bandopadhyay, R., Orte, C., Lawrenson, J.G., Reid, A.R., De Silva, S., and Allt, G. (2001). Contractile proteins in pericytes at the blood-brain and blood-retinal barriers. J. Neurocytol. *30*, 35–44.

Barrett, M.J.P., Tawhai, M.H., and Suresh, V. (2012). Arteries dominate volume changes during brief functional hyperemia: evidence from mathematical modelling. NeuroImage *62*, 482–492.

Bell, R.D., Winkler, E.A., Sagare, A.P., Singh, I., LaRue, B., Deane, R., and Zlokovic, B.V. (2010). Pericytes control key neurovascular functions and neuronal phenotype in the adult brain and during brain aging. Neuron *68*, 409–427.

Beltramo, E., and Porta, M. (2013). Pericyte loss in diabetic retinopathy: mechanisms and consequences. Curr. Med. Chem. *20*, 3218–3225.

Ben-nun J (1996). Comparative flow velocity of erythrocytes and leukocytes in feline retinal capillaries. Invest. Ophthalmol. Vis. Sci. *37*, 1854–1859.

Ben-nun J, Alder, V., Thompson, D., and Constable, I.J. (1992). Flow patterns of blood cells in the retinal capillaries. Retinal capillary flow patterns. Int. Ophthalmol. *16*, 81–89.

Bergua, A., Schrödl, F., and Neuhuber, W.L. (2003). Vasoactive intestinal and calcitonin gene-related peptides, tyrosine hydroxylase and nitrergic markers in the innervation of the rat central retinal artery. Exp. Eye Res. *77*, 367–374.

Bill, A., and Sperber, G.O. (1990). Aspects of oxygen and glucose consumption in the retina: effects of high intraocular pressure and light. Graefes Arch. Clin. Exp. Ophthalmol. Albrecht Von Graefes Arch. Für Klin. Exp. Ophthalmol. *228*, 124–127.

Bill, A., Sperber, G., and Ujiie, K. (1983). Physiology of the choroidal vascular bed. Int. Ophthalmol. *6*, 101–107.

Blinder, P., Tsai, P.S., Kaufhold, J.P., Knutsen, P.M., Suhl, H., and Kleinfeld, D. (2013). The cortical angiome: an interconnected vascular network with noncolumnar patterns of blood flow. Nat. Neurosci. *16*, 889–897.

Boado, R.J., and Pardridge, W.M. (1994). Differential expression of alpha-actin mRNA and immunoreactive protein in brain microvascular pericytes and smooth muscle cells. J. Neurosci. Res. *39*, 430–435.

Boas, D.A., Jones, S.R., Devor, A., Huppert, T.J., and Dale, A.M. (2008). A vascular anatomical network model of the spatio-temporal response to brain activation. NeuroImage *40*, 1116–1129.

Bonder, D.E., and McCarthy, K.D. (2014). Astrocytic Gq-GPCR-Linked IP3R-Dependent Ca2+ Signaling Does Not Mediate Neurovascular Coupling in Mouse Visual Cortex In Vivo. J. Neurosci. Off. J. Soc. Neurosci. *34*, 13139–13150.

Borysova, L., Wray, S., Eisner, D.A., and Burdyga, T. (2013). How calcium signals in myocytes and pericytes are integrated across in situ microvascular networks and control microvascular tone. Cell Calcium.

Buerk, D.G., Riva, C.E., and Cranstoun, S.D. (1995). Frequency and luminance-dependent blood flow and K+ ion changes during flicker stimuli in cat optic nerve head. Invest. Ophthalmol. Vis. Sci. *36*, 2216–2227.

Buxton, R.B. (2010). Interpreting oxygenation-based neuroimaging signals: the importance and the challenge of understanding brain oxygen metabolism. Front. Neuroenergetics *2*, 8.

Buxton, R.B., Griffeth, V.E.M., Simon, A.B., Moradi, F., and Shmuel, A. (2014). Variability of the coupling of blood flow and oxygen metabolism responses in the brain: a problem for interpreting BOLD studies but potentially a new window on the underlying neural activity. Front. Neurosci. *8*, 139.

Carroll, E.W., and Wong-Riley, M.T. (1984). Quantitative light and electron microscopic analysis of cytochrome oxidase-rich zones in the striate cortex of the squirrel monkey. J. Comp. Neurol. *222*, 1–17.

Cassot, F., Lauwers, F., Fouard, C., Prohaska, S., and Lauwers-Cances, V. (2006). A novel three-dimensional computer-assisted method for a quantitative study of microvascular networks of the human cerebral cortex. Microcirc. N. Y. N 1994 *13*, 1–18.

Cassot, F., Lauwers, F., Lorthois, S., Puwanarajah, P., and Duvernoy, H. (2009). Scaling laws for branching vessels of human cerebral cortex. Microcirc. N. Y. N 1994 *16*, 331–344, 2 p following 344.

Chaigneau, E., Oheim, M., Audinat, E., and Charpak, S. (2003). Two-photon imaging of capillary blood flow in olfactory bulb glomeruli. Proc. Natl. Acad. Sci. U. S. A. *100*, 13081–13086.

Chan-Ling, T. (1997). Glial, vascular, and neuronal cytogenesis in whole-mounted cat retina. Microsc. Res. Tech. *36*, 1–16.

Chan-Ling, T., Koina, M.E., McColm, J.R., Dahlstrom, J.E., Bean, E., Adamson, S., Yun, S., and Baxter, L. (2011). Role of CD44+ stem cells in mural cell formation in the human choroid: evidence of vascular instability due to limited pericyte ensheathment. Invest. Ophthalmol. Vis. Sci. *52*, 399–410.

Chen, Q., and Anderson, D.R. (1997). Effect of CO2 on intracellular pH and contraction of retinal capillary pericytes. Invest. Ophthalmol. Vis. Sci. *38*, 643–651.

Chen, B.R., Bouchard, M.B., McCaslin, A.F.H., Burgess, S.A., and Hillman, E.M.C. (2011). High-speed vascular dynamics of the hemodynamic response. NeuroImage *54*, 1021–1030.

Cheng, H., Nair, G., Walker, T.A., Kim, M.K., Pardue, M.T., Thulé, P.M., Olson, D.E., and Duong, T.Q. (2006). Structural and functional MRI reveals multiple retinal layers. Proc. Natl. Acad. Sci. U. S. A. *103*, 17525–17530.

Chhatbar, P.Y., and Kara, P. (2013). Improved blood velocity measurements with a hybrid image filtering and iterative Radon transform algorithm. Front. Neurosci. *7*, 106.

Choi, W., Baumann, B., Liu, J.J., Clermont, A.C., Feener, E.P., Duker, J.S., and Fujimoto, J.G. (2012). Measurement of pulsatile total blood flow in the human and rat retina with ultrahigh speed spectral/Fourier domain OCT. Biomed. Opt. Express *3*, 1047–1061.

Claudio, L., Raine, C.S., and Brosnan, C.F. (1995). Evidence of persistent blood-brain barrier abnormalities in chronic-progressive multiple sclerosis. Acta Neuropathol. (Berl.) *90*, 228–238.

Cogan, D.G., and Kuwabara, T. (1984). Comparison of retinal and cerebral vasculature in trypsin digest preparations. Br. J. Ophthalmol. *68*, 10–12.

Cogan, D.G., Toussant, D., and Kuwabara, T. (1961). Retinal vascular patterns. IV. Diabetic retinopathy. Arch. Ophthalmol. *66*, 366–378.

Collins, D.M., McCullough, W.T., and Ellsworth, M.L. (1998). Conducted vascular responses: communication across the capillary bed. Microvasc. Res. *56*, 43–53.

Dai, M., Nuttall, A., Yang, Y., and Shi, X. (2009). Visualization and contractile activity of cochlear pericytes in the capillaries of the spiral ligament. Hear. Res. *254*, 100–107.

Daneman, R., Zhou, L., Kebede, A.A., and Barres, B.A. (2010). Pericytes are required for blood-brain barrier integrity during embryogenesis. Nature *468*, 562–566.

Devor, A., Tian, P., Nishimura, N., Teng, I.C., Hillman, E.M.C., Narayanan, S.N., Ulbert, I., Boas, D.A., Kleinfeld, D., and Dale, A.M. (2007). Suppressed neuronal activity and concurrent arteriolar vasoconstriction may explain negative blood oxygenation level-dependent signal. J. Neurosci. Off. J. Soc. Neurosci. *27*, 4452–4459.

Devor, A., Sakadzic, S., Saisan, P.A., Yaseen, M.A., Roussakis, E., Srinivasan, V.J., Vinogradov, S.A., Rosen, B.R., Buxton, R.B., Dale, A.M., et al. (2011). "Overshoot" of O_2 is required to maintain baseline tissue oxygenation at locations distal to blood vessels. J. Neurosci. Off. J. Soc. Neurosci. *31*, 13676–13681.

Diaz-Flores, L., Gutierrez, R., Lopez-Alonso, A., Gonzalez, R., and Varela, H. (1992). Pericytes as a supplementary source of osteoblasts in periosteal osteogenesis. Clin. Orthop. 280–286.

Doblhoff-Dier, V., Schmetterer, L., Vilser, W., Garhöfer, G., Gröschl, M., Leitgeb, R.A., and Werkmeister, R.M. (2014). Measurement of the total retinal blood flow using dual beam Fourier-domain Doppler optical coherence tomography with orthogonal detection planes. Biomed. Opt. Express *5*, 630–642.

Dore-Duffy, P. (2008). Pericytes: pluripotent cells of the blood brain barrier. Curr. Pharm. Des. *14*, 1581–1593.

Dore-Duffy, P., and Cleary, K. (2011). Morphology and Properties of Pericytes. Methods Mol. Biol. Clifton NJ *686*, 49–68.

Dore-Duffy, P., Owen, C., Balabanov, R., Murphy, S., Beaumont, T., and Rafols, J.A. (2000). Pericyte migration from the vascular wall in response to traumatic brain injury. Microvasc. Res. *60*, 55–69.

Dore-Duffy, P., Katychev, A., Wang, X., and Van Buren, E. (2006). CNS microvascular pericytes exhibit multipotential stem cell activity. J. Cereb. Blood Flow Metab. Off. J. Int. Soc. Cereb. Blood Flow Metab. *26*, 613–624.

Dore-Duffy, P., Wang, S., Mehedi, A., Katyshev, V., Cleary, K., Tapper, A., Reynolds, C., Ding, Y., Zhan, P., Rafols, J., et al. (2011). Pericyte-mediated vasoconstriction underlies TBI-induced hypoperfusion. Neurol. Res. *33*, 176–186.

Dowling, J.E. (1968). Synaptic organization of the frog retina: an electron microscopic analysis comparing the retinas of frogs and primates. Proc. R. Soc. Lond. Ser. B Contain. Pap. Biol. Character R. Soc. G. B. *170*, 205–228.

Drew, P.J., Shih, A.Y., and Kleinfeld, D. (2011). Fluctuating and sensory-induced vasodynamics in rodent cortex extend arteriole capacity. Proc. Natl. Acad. Sci. U. S. A. *108*, 8473–8478.

Farrington-Rock, C., Crofts, N.J., Doherty, M.J., Ashton, B.A., Griffin-Jones, C., and Canfield, A.E. (2004). Chondrogenic and adipogenic potential of microvascular pericytes. Circulation *110*, 2226–2232.

Fernández-Klett, F., Offenhauser, N., Dirnagl, U., Priller, J., and Lindauer, U. (2010). Pericytes in capillaries are contractile in vivo, but arterioles mediate functional hyperemia in the mouse brain. Proc. Natl. Acad. Sci. U. S. A. *107*, 22290–22295.

Forster, B.A., Ferrari-Dileo, G., and Anderson, D.R. (1987). Adrenergic alpha 1 and alpha 2 binding sites are present in bovine retinal blood vessels. Invest. Ophthalmol. Vis. Sci. *28*, 1741–1746.

Frank, R.N., Dutta, S., and Mancini, M.A. (1987). Pericyte coverage is greater in the retinal than in the cerebral capillaries of the rat. Invest. Ophthalmol. Vis. Sci. *28*, 1086–1091.

Fung, Y.C. (1969). Blood flow in the capillary bed. J. Biomech. *2*, 353–372.

Furukawa, H. (1987). Autonomic innervation of preretinal blood vessels of the rabbit. Invest. Ophthalmol. Vis. Sci. *28*, 1752–1760.

Gaengel, K., Genové, G., Armulik, A., and Betsholtz, C. (2009). Endothelial-mural cell signaling in vascular development and angiogenesis. Arterioscler. Thromb. Vasc. Biol. *29*, 630–638.

Ganesan, P., He, S., and Xu, H. (2010). Development of an image-based network model of retinal vasculature. Ann. Biomed. Eng. *38*, 1566–1585.

Ganesan, P., He, S., and Xu, H. (2011). Development of an image-based model for capillary vasculature of retina. Comput. Methods Programs Biomed. *102*, 35–46.

Garcia, J.P.S., Jr, Garcia, P.T., and Rosen, R.B. (2002). Retinal blood flow in the normal human eye using the canon laser blood flowmeter. Ophthalmic Res. *34*, 295–299.

Garhöfer, G., Zawinka, C., Huemer, K.-H., Schmetterer, L., and Dorner, G.T. (2003). Flicker light-induced vasodilatation in the human retina: effect of lactate and changes in mean arterial pressure. Invest. Ophthalmol. Vis. Sci. *44*, 5309–5314.

Garhöfer, G., Zawinka, C., Resch, H., Huemer, K.H., Schmetterer, L., and Dorner, G.T. (2004a). Response of retinal vessel diameters to flicker stimulation in patients with early open angle glaucoma. J. Glaucoma *13*, 340–344.

Garhöfer, G., Zawinka, C., Resch, H., Huemer, K.H., Dorner, G.T., and Schmetterer, L. (2004b). Diffuse luminance flicker increases blood flow in major retinal arteries and veins. Vision Res. *44*, 833–838.

Garhofer, G., Werkmeister, R., Dragostinoff, N., and Schmetterer, L. (2012). Retinal blood flow in healthy young subjects. Invest. Ophthalmol. Vis. Sci. *53*, 698–703.

La Garza, B.H.D., Muir, E.R., Li, G., Shih, Y.-Y.I., and Duong, T.Q. (2010). Blood oxygenation level-dependent (BOLD) functional MRI of visual stimulation in the rat retina at 11.7 T. NMR Biomed.

Genevois, O., Paques, M., Simonutti, M., Sercombe, R., Seylaz, J., Gaudric, A., Brouland, J.-P., Sahel, J., and Vicaut, E. (2004). Microvascular remodeling after occlusion-recanalization of a branch retinal vein in rats. Invest. Ophthalmol. Vis. Sci. *45*, 594–600.

Gerhardt, H., and Betsholtz, C. (2003). Endothelial-pericyte interactions in angiogenesis. Cell Tissue Res. *314*, 15–23.

Gerrits, R.J., Raczynski, C., Greene, A.S., and Stein, E.A. (2000). Regional cerebral blood flow responses to variable frequency whisker stimulation: an autoradiographic analysis. Brain Res. *864*, 205–212.

Gilmore, E.D., Hudson, C., Preiss, D., and Fisher, J. (2005). Retinal arteriolar diameter, blood velocity, and blood flow response to an isocapnic hyperoxic provocation. Am. J. Physiol. Heart Circ. Physiol. *288*, H2912–H2917.

Goense, J., Merkle, H., and Logothetis, N.K. (2012). High-Resolution fMRI Reveals Laminar Differences in Neurovascular Coupling between Positive and Negative BOLD Responses. Neuron *76*, 629–639.

Guan, K., Hudson, C., and Flanagan, J.G. (2003). Variability and repeatability of retinal blood flow measurements using the Canon Laser Blood Flowmeter. Microvasc. Res. *65*, 145–151.

Guidoboni, G., Malgaroli, F., Causin, P., Sacco, R., Siesky, B., and Harris, A. (2014). Theoretical investigation of factors influencing oxygen levels in retinal vessels and tissue. (Orlando, FL),.

Hall, C.N., Reynell, C., Gesslein, B., Hamilton, N.B., Mishra, A., Sutherland, B.A., O'Farrell, F.M., Buchan, A.M., Lauritzen, M., and Attwell, D. (2014). Capillary pericytes regulate cerebral blood flow in health and disease. Nature *508*, 55–60.

Hamel, E. (2006). Perivascular nerves and the regulation of cerebrovascular tone. J. Appl. Physiol. Bethesda Md 1985 *100*, 1059–1064.

Hamilton, N.B., Attwell, D., and Hall, C.N. (2010). Pericyte-mediated regulation of capillary diameter: a component of neurovascular coupling in health and disease. Front. Neuroenergetics *2*.

Hammer, M., Vilser, W., Riemer, T., Liemt, F., Jentsch, S., Dawczynski, J., and Schweitzer, D. (2011). Retinal venous oxygen saturation increases by flicker light stimulation. Invest. Ophthalmol. Vis. Sci. *52*, 274–277.

Harel, N., Bolan, P.J., Turner, R., Ugurbil, K., and Yacoub, E. (2010). Recent Advances in High-Resolution MR Application and Its Implications for Neurovascular Coupling Research. Front. Neuroenergetics *2*, 130.

Haydon, P.G., and Carmignoto, G. (2006). Astrocyte control of synaptic transmission and neurovascular coupling. Physiol. Rev. *86*, 1009–1031.

Heinsen, H., and Heinsen, Y.L. (1983). Cerebellar capillaries. Qualitative and quantitative observations in young and senile rats. Anat. Embryol. (Berl.) *168*, 101–116.

Hellström, M., Gerhardt, H., Kalén, M., Li, X., Eriksson, U., Wolburg, H., and Betsholtz, C. (2001). Lack of pericytes leads to endothelial hyperplasia and abnormal vascular morphogenesis. J. Cell Biol. *153*, 543–553.

Herman, I.M., and Jacobson, S. (1988). In situ analysis of microvascular pericytes in hypertensive rat brains. Tissue Cell *20*, 1–12.

Hinz, B., Celetta, G., Tomasek, J.J., Gabbiani, G., and Chaponnier, C. (2001). Alpha-smooth muscle actin expression upregulates fibroblast contractile activity. Mol. Biol. Cell *12*, 2730–2741.

Hirsch, S., Reichold, J., Schneider, M., Székely, G., and Weber, B. (2012). Topology and hemodynamics of the cortical cerebrovascular system. J. Cereb. Blood Flow Metab. Off. J. Int. Soc. Cereb. Blood Flow Metab. *32*, 952–967.

Huber, L., Goense, J., Kennerley, A.J., Trampel, R., Guidi, M., Reimer, E., Ivanov, D., Neef, N., Gauthier, C.J., Turner, R., et al. (2014). Cortical lamina-dependent blood volume changes in human brain at 7T. NeuroImage.

Hudetz, A.G., Fehér, G., Weigle, C.G., Knuese, D.E., and Kampine, J.P. (1995). Video microscopy of cerebrocortical capillary flow: response to hypotension and intracranial hypertension. Am. J. Physiol. *268*, H2202–H2210.

Hughes, S., and Chan-Ling, T. (2004). Characterization of smooth muscle cell and pericyte differentiation in the rat retina in vivo. Invest. Ophthalmol. Vis. Sci. *45*, 2795–2806.

Huppert, T.J., Allen, M.S., Benav, H., Jones, P.B., and Boas, D.A. (2007). A multicompartment vascular model for inferring baseline and functional changes in cerebral oxygen metabolism and arterial dilation. J. Cereb. Blood Flow Metab. Off. J. Int. Soc. Cereb. Blood Flow Metab. *27*, 1262–1279.

Hutchinson, E.B., Stefanovic, B., Koretsky, A.P., and Silva, A.C. (2006). Spatial flow-volume dissociation of the cerebral microcirculatory response to mild hypercapnia. NeuroImage *32*, 520–530.

Iadecola, C., and Nedergaard, M. (2007). Glial regulation of the cerebral microvasculature. Nat. Neurosci. *10*, 1369–1376.

Ishizaki, E., Fukumoto, M., and Puro, D.G. (2009). Functional K(ATP) channels in the rat retinal microvasculature: topographical distribution, redox regulation, spermine modulation and diabetic alteration. J. Physiol. *587*, 2233–2253.

Ivanova, E., Toychiev, A.H., Yee, C.W., and Sagdullaev, B.T. (2014). Intersublaminar vascular plexus: the correlation of retinal blood vessels with functional sublaminae of the inner plexiform layer. Invest. Ophthalmol. Vis. Sci. *55*, 78–86.

Joyce, N.C., Haire, M.F., and Palade, G.E. (1985). Contractile proteins in pericytes. I. Immunoperoxidase localization of tropomyosin. J. Cell Biol. *100*, 1379–1386.

Kamouchi, M., Kitazono, T., Ago, T., Wakisaka, M., Ooboshi, H., Ibayashi, S., and Iida, M. (2004). Calcium influx pathways in rat CNS pericytes. Brain Res. Mol. Brain Res. *126*, 114–120.

Kamoun, W.S., Chae, S.-S., Lacorre, D.A., Tyrrell, J.A., Mitre, M., Gillissen, M.A., Fukumura, D., Jain, R.K., and Munn, L.L. (2010). Simultaneous measurement of RBC velocity, flux, hematocrit and shear rate in vascular networks. Nat. Methods *7*, 655–660.

Kassab, G.S., Berkley, J., and Fung, Y.C. (1997). Analysis of pig's coronary arterial blood flow with detailed anatomical data. Ann. Biomed. Eng. *25*, 204–217.

Kawamura, H., Oku, H., Li, Q., Sakagami, K., and Puro, D.G. (2002). Endothelin-induced changes in the physiology of retinal pericytes. Invest. Ophthalmol. Vis. Sci. *43*, 882–888.

Kawamura, H., Kobayashi, M., Li, Q., Yamanishi, S., Katsumura, K., Minami, M., Wu, D.M., and Puro, D.G. (2004). Effects of angiotensin II on the pericyte-containing microvasculature of the rat retina. J. Physiol. *561*, 671–683.

Kennerley, A.J., Mayhew, J.E., Redgrave, P., and Berwick, J. (2010). Vascular Origins of BOLD and CBV fMRI Signals: Statistical Mapping and Histological Sections Compared. Open Neuroimaging J. *4*, 1–8.

Khoobehi, B., Peyman, G.A., Carnahan, L.G., and Hayes, R.L. (2003). A novel approach for freeze-frame video determination of volumetric blood flow in the rat retina. Ophthalmic Surg. Lasers Imaging Off. J. Int. Soc. Imaging Eye *34*, 505–514.

Kim, T., and Kim, S.-G. (2010). Cortical layer-dependent arterial blood volume changes: improved spatial specificity relative to BOLD fMRI. NeuroImage *49*, 1340–1349.

Kim, J.H., Kim, J.H., Yu, Y.S., Kim, D.H., and Kim, K.-W. (2009). Recruitment of pericytes and astrocytes is closely related to the formation of tight junction in developing retinal vessels. J. Neurosci. Res. *87*, 653–659.

Kim, T.N., Goodwill, P.W., Chen, Y., Conolly, S.M., Schaffer, C.B., Liepmann, D., and Wang, R.A. (2012). Line-scanning particle image velocimetry: an optical approach for quantifying a wide range of blood flow speeds in live animals. PloS One *7*, e38590.

Kleinfeld, D., Mitra, P.P., Helmchen, F., and Denk, W. (1998). Fluctuations and stimulus-induced changes in blood flow observed in individual capillaries in layers 2 through 4 of rat neocortex. Proc. Natl. Acad. Sci. U. S. A. *95*, 15741–15746.

Kong, Y., Zheng, Y., Johnston, D., Martindale, J., Jones, M., Billings, S., and Mayhew, J. (2004). A model of the dynamic relationship between blood flow and volume changes during brain activation. J. Cereb. Blood Flow Metab. Off. J. Int. Soc. Cereb. Blood Flow Metab. *24*, 1382–1392.

Kornfield, T.E., and Newman, E.A. (2014). Regulation of blood flow in the retinal trilaminar vascular network. J. Neurosci. Off. J. Soc. Neurosci. *34*, 11504–11513.

Kotecki, M., Zeiger, A.S., Van Vliet, K.J., and Herman, I.M. (2010). Calpain- and talin-dependent control of microvascular pericyte contractility and cellular stiffness. Microvasc. Res. *80*, 339–348.

Krolo, I., and Hudetz, A.G. (2000). Hypoxemia alters erythrocyte perfusion pattern in the cerebral capillary network. Microvasc. Res. *59*, 72–79.

Krueger, M., and Bechmann, I. (2010). CNS pericytes: concepts, misconceptions, and a way out. Glia *58*, 1–10.

Kunz, J., Krause, D., Gehrmann, J., and Dermietzel, R. (1995). Changes in the expression pattern of blood-brain barrier-associated pericytic aminopeptidase N (pAP N) in the course of acute experimental autoimmune encephalomyelitis. J. Neuroimmunol. *59*, 41–55.

Lacar, B., Herman, P., Hartman, N.W., Hyder, F., and Bordey, A. (2012). S phase entry of neural progenitor cells correlates with increased blood flow in the young subventricular zone. PloS One *7*, e31960.

Lanigan, L.P., Birche, R., Clark, C.V., and Hill, D.W. (1990). The effect of cervical sympathectomy on retinal vessel responses to systemic autonomic stimulation. Eye Lond. Engl. *4 (Pt 1)*, 181–189.

Lapi, D., Marchiafava, P.L., and Colantuoni, A. (2008). Geometric characteristics of arterial network of rat pial microcirculation. J. Vasc. Res. *45*, 69–77.

Lau, J.C.M., and Linsenmeier, R.A. (2012). Oxygen consumption and distribution in the Long-Evans rat retina. Exp. Eye Res.

Leitgeb, R.A., Werkmeister, R.M., Blatter, C., and Schmetterer, L. (2014). Doppler optical coherence tomography. Prog. Retin. Eye Res. *41*, 26–43.

Leskova, W., Watts, M.N., Carter, P.R., Eshaq, R.S., and Harris, N.R. (2013). Measurement of retinal blood flow rate in diabetic rats: disparity between techniques due to redistribution of flow. Invest. Ophthalmol. Vis. Sci. *54*, 2992–2999.

Li, Q., and Puro, D.G. (2001). Adenosine activates ATP-sensitive K(+) currents in pericytes of rat retinal microvessels: role of A1 and A2a receptors. Brain Res. *907*, 93–99.

Lindvere, L., Janik, R., Dorr, A., Chartash, D., Sahota, B., Sled, J.G., and Stefanovic, B. (2013). Cerebral microvascular network geometry changes in response to functional stimulation. NeuroImage *71*, 248–259.

Linsenmeier, R.A. (1986). Effects of light and darkness on oxygen distribution and consumption in the cat retina. J. Gen. Physiol. *88*, 521–542.

Linsenmeier, R.A., and Padnick-Silver, L. (2000). Metabolic dependence of photoreceptors on the choroid in the normal and detached retina. Invest. Ophthalmol. Vis. Sci. *41*, 3117–3123.

Liwnicz, B.H., Leach, J.L., Yeh, H.S., and Privitera, M. (1990). Pericyte degeneration and thickening of basement membranes of cerebral microvessels in complex partial seizures: electron microscopic study of surgically removed tissue. Neurosurgery *26*, 409–420.

Logean, Eric, and Schmetterer, L. (2003). Velocity profile of red blood cells in human retinal vessels using confocal scanning laser Doppler velocimetry. Laser Phys. *13*, 45–51.

Lorentz, K., Zayas-Santiago, A., Tummala, S., and Kang Derwent, J.J. (2008). Scanning laser ophthalmoscope-particle tracking method to assess blood velocity during hypoxia and hyperoxia. Adv. Exp. Med. Biol. *614*, 253–261.

Lorthois, S., and Cassot, F. (2010). Fractal analysis of vascular networks: insights from morphogenesis. J. Theor. Biol. *262*, 614–633.

Mandeville, J.B., Marota, J.J., Ayata, C., Zaharchuk, G., Moskowitz, M.A., Rosen, B.R., and Weisskoff, R.M. (1999). Evidence of a cerebrovascular postarteriole windkessel with delayed compliance. J. Cereb. Blood Flow Metab. Off. J. Int. Soc. Cereb. Blood Flow Metab. *19*, 679–689.

Mathiisen, T.M., Lehre, K.P., Danbolt, N.C., and Ottersen, O.P. (2010). The perivascular astroglial sheath provides a complete covering of the brain microvessels: an electron microscopic 3D reconstruction. Glia *58*, 1094–1103.

Miller, R. (2001). The physiology and morphology of the vertebrate retina. In Retina, S. Ryan, ed. (St. Louis: Mosby), pp. 138–170.

Mishra, A., and Newman, E.A. (2011). Aminoguanidine reverses the loss of functional hyperemia in a rat model of diabetic retinopathy. Front. Neuroenergetics *3*, 10.

Mishra, A., Clark, B.D., Hamid, A., and Newman, E.A. (2010). Oxygen Modulated Neurovascular Coupling in the Retina. (San Diego, CA),.

Mishra, A., O'Farrell, F.M., Reynell, C., Hamilton, N.B., Hall, C.N., and Attwell, D. (2014). Imaging pericytes and capillary diameter in brain slices and isolated retinae. Nat. Protoc. *9*, 323–336.

Mosso, A. (1880). Sulla circolazione del sangue nel cervello dell'uomo: ricerche sfigmografiche (Salviucci).

Nehls, V., and Drenckhahn, D. (1991). Heterogeneity of microvascular pericytes for smooth muscle type alpha-actin. J. Cell Biol. *113*, 147–154.

Newman, E.A. (2005). Calcium increases in retinal glial cells evoked by light-induced neuronal activity. J. Neurosci. Off. J. Soc. Neurosci. *25*, 5502–5510.

Newman, E.A. (2013). Functional hyperemia and mechanisms of neurovascular coupling in the retinal vasculature. J. Cereb. Blood Flow Metab. Off. J. Int. Soc. Cereb. Blood Flow Metab.

Nizar, K., Uhlirova, H., Tian, P., Saisan, P.A., Cheng, Q., Reznichenko, L., Weldy, K.L., Steed, T.C., Sridhar, V.B., Macdonald, C.L., et al. (2013). In vivo Stimulus-Induced Vasodilation Occurs without IP3 Receptor Activation and May Precede Astrocytic Calcium Increase. J. Neurosci. Off. J. Soc. Neurosci. *33*, 8411–8422.

Noonan, J.E., Nguyen, T.T., Man, R.E.K., Best, W.J., Wang, J.J., and Lamoureux, E.L. (2013). Retinal arteriolar dilation to flicker light is reduced on short-term retesting. Invest. Ophthalmol. Vis. Sci. *54*, 7764–7768.

Norup Nielsen, A., and Lauritzen, M. (2001). Coupling and uncoupling of activity-dependent increases of neuronal activity and blood flow in rat somatosensory cortex. J. Physiol. *533*, 773–785.

Paques, M., Tadayoni, R., Sercombe, R., Laurent, P., Genevois, O., Gaudric, A., and Vicaut, E. (2003). Structural and hemodynamic analysis of the mouse retinal microcirculation. Invest. Ophthalmol. Vis. Sci. *44*, 4960–4967.

Parpaleix, A., Houssen, Y.G., and Charpak, S. (2013). Imaging local neuronal activity by monitoring PO_2 transients in capillaries. Nat. Med. *19*, 241–246.

Parthasarathi, A.A., Japee, S.A., and Pittman, R.N. (1999). Determination of red blood cell velocity by video shuttering and image analysis. Ann. Biomed. Eng. *27*, 313–325.

Paulson, O.B., Hasselbalch, S.G., Rostrup, E., Knudsen, G.M., and Pelligrino, D. (2010). Cerebral blood flow response to functional activation. J. Cereb. Blood Flow Metab. Off. J. Int. Soc. Cereb. Blood Flow Metab. *30*, 2–14.

Peppiatt, C.M., Howarth, C., Mobbs, P., and Attwell, D. (2006). Bidirectional control of CNS capillary diameter by pericytes. Nature *443*, 700–704.

Perea, G., Navarrete, M., and Araque, A. (2009). Tripartite synapses: astrocytes process and control synaptic information. Trends Neurosci. *32*, 421–431.

Pieper, C., Marek, J.J., Unterberg, M., Schwerdtle, T., and Galla, H.-J. (2014). Brain capillary pericytes contribute to the immune defense in response to cytokines or LPS in vitro. Brain Res. *1550*, 1–8.

Pinard, E., Nallet, H., MacKenzie, E.T., Seylaz, J., and Roussel, S. (2002). Penumbral microcirculatory changes associated with peri-infarct depolarizations in the rat. Stroke J. Cereb. Circ. *33*, 606–612.

Polak, K., Schmetterer, L., and Riva, C.E. (2002). Influence of flicker frequency on flicker-induced changes of retinal vessel diameter. Invest. Ophthalmol. Vis. Sci. *43*, 2721–2726.

Pournaras, C.J., and Riva, C.E. (2013). Retinal blood flow evaluation. Ophthalmol. J. Int. Ophtalmol. Int. J. Ophthalmol. Z. Für Augenheilkd. *229*, 61–74.

Provis, J.M. (2001). Development of the primate retinal vasculature. Prog. Retin. Eye Res. *20*, 799–821.

Puro, D.G. (2007). Physiology and pathobiology of the pericyte-containing retinal microvasculature: new developments. Microcirc. N. Y. N 1994 *14*, 1–10.

Raichle, M.E. (1998). Behind the scenes of functional brain imaging: a historical and physiological perspective. Proc. Natl. Acad. Sci. U. S. A. *95*, 765–772.

Reichold, J., Stampanoni, M., Lena Keller, A., Buck, A., Jenny, P., and Weber, B. (2009). Vascular graph model to simulate the cerebral blood flow in realistic vascular networks. J. Cereb. Blood Flow Metab. Off. J. Int. Soc. Cereb. Blood Flow Metab. *29*, 1429–1443.

Reitsma, S., Slaaf, D.W., Vink, H., van Zandvoort, M.A.M.J., and oude Egbrink, M.G.A. (2007). The endothelial glycocalyx: composition, functions, and visualization. Pflüg. Arch. Eur. J. Physiol. *454*, 345–359.

Reyes-Aldasoro, C.C., Akerman, S., and Tozer, G.M. (2008). Measuring the velocity of fluorescently labelled red blood cells with a keyhole tracking algorithm. J. Microsc. *229*, 162–173.

Risser, L., Plouraboué, F., Steyer, A., Cloetens, P., Le Duc, G., and Fonta, C. (2007). From homogeneous to fractal normal and tumorous microvascular networks in the brain. J. Cereb. Blood Flow Metab. Off. J. Int. Soc. Cereb. Blood Flow Metab. *27*, 293–303.

Riva, C.E., Grunwald, J.E., Sinclair, S.H., and Petrig, B.L. (1985). Blood velocity and volumetric flow rate in human retinal vessels. Invest. Ophthalmol. Vis. Sci. *26*, 1124–1132.

Rovainen, C.M., Woolsey, T.A., Blocher, N.C., Wang, D.B., and Robinson, O.F. (1993). Blood flow in single surface arterioles and venules on the mouse somatosensory cortex measured with videomicroscopy, fluorescent dextrans, nonoccluding fluorescent beads, and computer-assisted image analysis. J. Cereb. Blood Flow Metab. Off. J. Int. Soc. Cereb. Blood Flow Metab. *13*, 359–371.

Roy, C.S., and Sherrington, C.S. (1890). On the Regulation of the Blood-supply of the Brain. J. Physiol. *11*, 85–158.17.

Santisakultarm, T.P., Cornelius, N.R., Nishimura, N., Schafer, A.I., Silver, R.T., Doerschuk, P.C., Olbricht, W.L., and Schaffer, C.B. (2012). In vivo two-photon excited fluorescence microscopy reveals cardiac- and respiration-dependent pulsatile blood flow in cortical blood vessels in mice. Am. J. Physiol. Heart Circ. Physiol. *302*, H1367–H1377.

Sarelius, I.H., and Duling, B.R. (1982). Direct measurement of microvessel hematocrit, red cell flux, velocity, and transit time. Am. J. Physiol. *243*, H1018–H1026.

Schaffer, C.B., Friedman, B., Nishimura, N., Schroeder, L.F., Tsai, P.S., Ebner, F.F., Lyden, P.D., and Kleinfeld, D. (2006). Two-photon imaging of cortical surface microvessels reveals a robust redistribution in blood flow after vascular occlusion. PLoS Biol. *4*, e22.

Schallek, J.B., Geng, Y., Nguyen, H., and Williams, D.R. (2013). Morphology and topography of retinal pericytes in the living mouse retina using in vivo adaptive optics imaging and ex vivo characterization. Invest. Ophthalmol. Vis. Sci.

Schildmeyer, L.A., Braun, R., Taffet, G., Debiasi, M., Burns, A.E., Bradley, A., and Schwartz, R.J. (2000). Impaired vascular contractility and blood pressure homeostasis in the smooth muscle alpha-actin null mouse. FASEB J. Off. Publ. Fed. Am. Soc. Exp. Biol. *14*, 2213–2220.

Schönfelder, U., Hofer, A., Paul, M., and Funk, R.H. (1998). In situ observation of living pericytes in rat retinal capillaries. Microvasc. Res. *56*, 22–29.

Schulte, M.L., Wood, J.D., and Hudetz, A.G. (2003). Cortical electrical stimulation alters erythrocyte perfusion pattern in the cerebral capillary network of the rat. Brain Res. *963*, 81–92.

Sehi, M., Tsui, E., Cheng, R., Wan, J., Wong, T., Dorner, S., Fisher, J., and Hudson, C. (2012). Relative magnitude of vascular reactivity in the major arterioles of the retina. Microvasc. Res. *83*, 200–204.

Seylaz, J., Charbonné, R., Nanri, K., Von Euw, D., Borredon, J., Kacem, K., Méric, P., and Pinard, E. (1999). Dynamic in vivo measurement of erythrocyte velocity and flow in capillaries and of microvessel diameter in the rat brain by confocal laser microscopy. J. Cereb. Blood Flow Metab. Off. J. Int. Soc. Cereb. Blood Flow Metab. *19*, 863–870.

Shahidi, A.M., Patel, S.R., Huang, D., Tan, O., Flanagan, J.G., and Hudson, C. (2014). Assessment of total retinal blood flow using Doppler Fourier Domain Optical Coherence Tomography during systemic hypercapnia and hypocapnia. Physiol. Rep. *2*.

Shahidi, M., Shakoor, A., Blair, N.P., Mori, M., and Shonat, R.D. (2006). A method for chorioretinal oxygen tension measurement. Curr. Eye Res. *31*, 357–366.

Shahidi, M., Wanek, J., Blair, N.P., and Mori, M. (2009). Three-dimensional mapping of chorioretinal vascular oxygen tension in the rat. Invest. Ophthalmol. Vis. Sci. *50*, 820–825.

Silva, A.C., and Koretsky, A.P. (2002). Laminar specificity of functional MRI onset times during somatosensory stimulation in rat. Proc. Natl. Acad. Sci. U. S. A. *99*, 15182–15187.

Smirnakis, S.M., Schmid, M.C., Weber, B., Tolias, A.S., Augath, M., and Logothetis, N.K. (2007). Spatial specificity of BOLD versus cerebral blood volume fMRI for mapping cortical organization. J. Cereb. Blood Flow Metab. Off. J. Int. Soc. Cereb. Blood Flow Metab. *27*, 1248–1261.

Srienc, A.I., Kurth-Nelson, Z.L., and Newman, E.A. (2010). Imaging retinal blood flow with laser speckle flowmetry. Front. Neuroenergetics *2*.

Srienc, A.I., Kornfield, T.E., Mishra, A., Burian, M.A., and Newman, E.A. (2012). Assessment of glial function in the in vivo retina. Methods Mol. Biol. Clifton NJ *814*, 499–514.

Stahl, A., Connor, K.M., Sapieha, P., Chen, J., Dennison, R.J., Krah, N.M., Seaward, M.R., Willett, K.L., Aderman, C.M., Guerin, K.I., et al. (2010). The mouse retina as an angiogenesis model. Invest. Ophthalmol. Vis. Sci. *51*, 2813–2826.

Takata, N., Nagai, T., Ozawa, K., Oe, Y., Mikoshiba, K., and Hirase, H. (2013). Cerebral blood flow modulation by Basal forebrain or whisker stimulation can occur independently of large cytosolic Ca2+ signaling in astrocytes. PloS One *8*, e66525.

Tan, P.E.Z., Yu, P.K., Balaratnasingam, C., Cringle, S.J., Morgan, W.H., McAllister, I.L., and Yu, D.-Y. (2012). Quantitative confocal imaging of the retinal microvasculature in the human retina. Invest. Ophthalmol. Vis. Sci. *53*, 5728–5736.

Tayyari, F., Yusof, F., Vymyslicky, M., Tan, O., Huang, D., Flanagan, J.G., and Hudson, C. (2014). Variability and Repeatability of Quantitative, Fourier Domain-OCT Doppler Blood Flow in Young and Elderly Healthy Subjects. Invest. Ophthalmol. Vis. Sci.

Tian, P., Teng, I.C., May, L.D., Kurz, R., Lu, K., Scadeng, M., Hillman, E.M.C., De Crespigny, A.J., D'Arceuil, H.E., Mandeville, J.B., et al. (2010). Cortical depth-specific microvascular dilation underlies laminar differences in blood oxygenation level-dependent functional MRI signal. Proc. Natl. Acad. Sci. U. S. A. *107*, 15246–15251.

Tomasek, J.J., Haaksma, C.J., Schwartz, R.J., Vuong, D.T., Zhang, S.X., Ash, J.D., Ma, J., and Al-Ubaidi, M.R. (2006). Deletion of smooth muscle alpha-actin alters blood-retina barrier permeability and retinal function. Invest. Ophthalmol. Vis. Sci. *47*, 2693–2700.

Tomita, M., Tomita, Y., Unekawa, M., Toriumi, H., and Suzuki, N. (2011). Oscillating neuro-capillary coupling during cortical spreading depression as observed by tracking of FITC-labeled RBCs in single capillaries. NeuroImage *56*, 1001–1010.

Unthank, J.L., Lash, J.M., Nixon, J.C., Sidner, R.A., and Bohlen, H.G. (1993). Evaluation of carbocyanine-labeled erythrocytes for microvascular measurements. Microvasc. Res. *45*, 193–210.

Vanzetta, I., Hildesheim, R., and Grinvald, A. (2005). Compartment-resolved imaging of activity-dependent dynamics of cortical blood volume and oximetry. J. Neurosci. Off. J. Soc. Neurosci. *25*, 2233–2244.

Verbeek, M.M., Otte-Höller, I., Wesseling, P., Ruiter, D.J., and de Waal, R.M. (1994). Induction of alpha-smooth muscle actin expression in cultured human brain pericytes by transforming growth factor-beta 1. Am. J. Pathol. *144*, 372–382.

Verbeek, M.M., de Waal, R.M., Schipper, J.J., and Van Nostrand, W.E. (1997). Rapid degeneration of cultured human brain pericytes by amyloid beta protein. J. Neurochem. *68*, 1135–1141.

Villringer, A., Them, A., Lindauer, U., Einhäupl, K., and Dirnagl, U. (1994). Capillary perfusion of the rat brain cortex. An in vivo confocal microscopy study. Circ. Res. *75*, 55–62.

Wajer, S.D., Taomoto, M., McLeod, D.S., McCally, R.L., Nishiwaki, H., Fabry, M.E., Nagel, R.L., and Lutty, G.A. (2000). Velocity measurements of normal and sickle red blood cells in the rat retinal and choroidal vasculatures. Microvasc. Res. *60*, 281–293.

Wanek, J., Teng, P.-Y., Albers, J., Blair, N.P., and Shahidi, M. (2011). Inner retinal metabolic rate of oxygen by oxygen tension and blood flow imaging in rat. Biomed. Opt. Express *2*, 2562–2568.

Wang, Y., Bower, B.A., Izatt, J.A., Tan, O., and Huang, D. (2007). In vivo total retinal blood flow measurement by Fourier domain Doppler optical coherence tomography. J. Biomed. Opt. *12*, 041215.

Wang, Y., Lu, A., Gil-Flamer, J., Tan, O., Izatt, J.A., and Huang, D. (2009). Measurement of total blood flow in the normal human retina using Doppler Fourier-domain optical coherence tomography. Br. J. Ophthalmol. *93*, 634–637.

Wang, Z., Yadav, A.S., Leskova, W., and Harris, N.R. (2011). Inhibition of 20-HETE attenuates diabetes-induced decreases in retinal hemodynamics. Exp. Eye Res. *93*, 108–113.

Webb, R.C. (2003). Smooth muscle contraction and relaxation. Adv. Physiol. Educ. *27*, 201–206.

Weber, B., Keller, A.L., Reichold, J., and Logothetis, N.K. (2008). The microvascular system of the striate and extrastriate visual cortex of the macaque. Cereb. Cortex N. Y. N 1991 *18*, 2318–2330.

Wilhelmus, M.M.M., Otte-Höller, I., van Triel, J.J.J., Veerhuis, R., Maat-Schieman, M.L.C., Bu, G., de Waal, R.M.W., and Verbeek, M.M. (2007). Lipoprotein receptor-related protein-1 mediates amyloid-beta-mediated cell death of cerebrovascular cells. Am. J. Pathol. *171*, 1989–1999.

Willerslev, A., Li, X.Q., Munch, I.C., and Larsen, M. (2014). Flow patterns on spectral-domain optical coherence tomography reveal flow directions at retinal vessel bifurcations. Acta Ophthalmol. (Copenh.) *92*, 461–464.

Winkler, E.A., Sengillo, J.D., Bell, R.D., Wang, J., and Zlokovic, B.V. (2012). Blood-spinal cord barrier pericyte reductions contribute to increased capillary permeability. J. Cereb. Blood Flow Metab. Off. J. Int. Soc. Cereb. Blood Flow Metab. *32*, 1841–1852.

Winkler, F., Kozin, S.V., Tong, R.T., Chae, S.-S., Booth, M.F., Garkavtsev, I., Xu, L., Hicklin, D.J., Fukumura, D., di Tomaso, E., et al. (2004). Kinetics of vascular normalization by VEGFR2 blockade governs brain tumor response to radiation: role of oxygenation, angiopoietin-1, and matrix metalloproteinases. Cancer Cell *6*, 553–563.

Wright, W.S., and Harris, N.R. (2008). Ozagrel attenuates early streptozotocin-induced constriction of arterioles in the mouse retina. Exp. Eye Res. *86*, 528–536.

Wu, D.M., Kawamura, H., Sakagami, K., Kobayashi, M., and Puro, D.G. (2003). Cholinergic regulation of pericyte-containing retinal microvessels. Am. J. Physiol. Heart Circ. Physiol. *284*, H2083–H2090.

Wu, D.M., Minami, M., Kawamura, H., and Puro, D.G. (2006). Electrotonic transmission within pericyte-containing retinal microvessels. Microcirc. N. Y. N 1994 *13*, 353–363.

Yamaguchi, S., Yamakawa, T., and Niimi, H. (1992). Red cell velocity and microvessel diameter measurement by a two fluorescent tracer method under epifluorescence microscopy: application to cerebral microvessels of cats. Int. J. Microcirc. Clin. Exp. Spons. Eur. Soc. Microcirc. *11*, 403–416.

Yamanishi, S., Katsumura, K., Kobayashi, T., and Puro, D.G. (2006). Extracellular lactate as a dynamic vasoactive signal in the rat retinal microvasculature. Am. J. Physiol. Heart Circ. Physiol. *290*, H925–H934.

Yazdanfar, S., Rollins, A.M., and Izatt, J.A. (2003). In vivo imaging of human retinal flow dynamics by color Doppler optical coherence tomography. Arch. Ophthalmol. *121*, 235–239.

Ye, X.D., Laties, A.M., and Stone, R.A. (1990). Peptidergic innervation of the retinal vasculature and optic nerve head. Invest. Ophthalmol. Vis. Sci. *31*, 1731–1737.

Yemisci, M., Gursoy-Ozdemir, Y., Vural, A., Can, A., Topalkara, K., and Dalkara, T. (2009). Pericyte contraction induced by oxidative-nitrative stress impairs capillary reflow despite successful opening of an occluded cerebral artery. Nat. Med. *15*, 1031–1037.

Yu, D.Y., and Cringle, S.J. (2001). Oxygen distribution and consumption within the retina in vascularised and avascular retinas and in animal models of retinal disease. Prog. Retin. Eye Res. *20*, 175–208.

Yu, D.Y., Cringle, S.J., Alder, V.A., and Su, E.N. (1994). Intraretinal oxygen distribution in rats as a function of systemic blood pressure. Am. J. Physiol. *267*, H2498–H2507.

Zhang, T., Wu, D.M., Xu, G.-Z., and Puro, D.G. (2011). The electrotonic architecture of the retinal microvasculature: modulation by angiotensin II. J. Physiol. *589*, 2383–2399.

Zhi, Z., Cepurna, W., Johnson, E., Shen, T., Morrison, J., and Wang, R.K. (2011). Volumetric and quantitative imaging of retinal blood flow in rats with optical microangiography. Biomed. Opt. Express *2*, 579–591.

Zhong, Z., Song, H., Chui, T.Y.P., Petrig, B.L., and Burns, S.A. (2011). Noninvasive measurements and analysis of blood velocity profiles in human retinal vessels. Invest. Ophthalmol. Vis. Sci. *52*, 4151–4157.

Zimmerhackl, B., Parekh, N., Brinkhus, H., and Steinhausen, M. (1983). The use of fluorescent labeled erythrocytes for intravital investigation of flow and local hematocrit in glomerular capillaries in the rat. Int. J. Microcirc. Clin. Exp. Spons. Eur. Soc. Microcirc. *2*, 119–129.